藥學 博士 學位 論文

Study on structural mechanism of activation by calcium of Anoctamin 1 (ANO1)/TMEM16A, calcium activated chloride channel

칼슘의존성염소이온채널인 Anoctamin 1의 칼슘 활성화에 대한 구조기반 기전연구

2017 年 2 月

서울大學校 大學院

藥學科 病態生理學 專攻

李 濟 宣

Study on structural mechanism of activation by calcium of Anoctamin 1 (ANO1)/TMEM16A, calcium activated chloride channel

칼슘의존성염소이온채널인 Anoctamin 1 의 칼슘 활성화에 대한 구조기반 기전연구

指導敎授 愼英基

이 論文을 藥學博士 學位論文으로 提出함

2016 年 12 月

서울大學校 大學院

藥學科 病態生理學專攻

李 濟 宣

李 濟 宣 의 藥學博士 學位論文을 認准함

2016 年 12 月

委 員 長 _____ (인)

副委員長 _____ (인)

委 員 _____ (인)

委 員 _____ (인)

委 員 _____ (인)

Abstract

Anoctamin 1 (ANO1)/TMEM16A is a key molecule known for contributing to a variety of physiological phenomena, playing a role as calcium activated chloride channel (CaCC). Despite of the importance of the activation of ANO1 by Ca^{2+}, it is still ambiguous to identify where Ca^{2+} binds to a region of ANO1 and to understand how to be activated by calcium. Here, we demonstrate that Ca^{2+} directly binds to the third intracellular loop (ICL3) of the ANO1 and two helices, "reference" and "Ca^{2+} sensor" helices in the ICL3 interact directly in a Ca^{2+} dependent manner as facing each other with opposite charges. Moreover neutralization or deletion of the negatively and positively charged residues in the two helices significantly changes the Ca^{2+} sensitivity of the ANO1. Therefore we predict a new activation mechanism by which the Ca^{2+} sensor helix attaches to the reference helix in the resting state, and as intracellular Ca^{2+} rises, Ca^{2+} acts on the sensor helix, which repels it from the reference helix. This Ca^{2+}-dependent push-pull conformational change would be a key electromechanical movement for gating the ANO1 channel.

Keywords: Anoctamin 1 (ANO1)/TMEM16A; Ca^{2+}; The third intracellular loop (ICL3); Ca^{2+} sensor helix; reference helix;

Student number: 2007-21860

Table of Contents

List of Figures

Introduction

1. Calcium Activated Chloride Channel (CaCC)

1.1 Physiological role of CaCCs

Cl^- channels are membrane proteins that play a role for a variety of cellular functions with the passive flow of Cl^- into and out of the cell. Among the several Cl^- channels, CaCCs are responsible for propagation of the action potential in neuronal cells, the flow of water out of secretory cells, as activated by cytosolic Ca^{2+} concentration ($[Ca^{2+}]_i$) (Hartzell. et al., 2005). $[Ca^{2+}]_i$ is originated from receptor-mediated (adrenergic, histaminergic, and cholinergic) Ca2+ mobilization (Pacaud et al., 1989; Wang et al., 1993) or from Ca2+ influx through voltage-dependent Ca2+ channels (Pacaud et al., 1989; Saleh et al. 2005). The direction of Cl^- movement through CaCCs is dictated by three factors such as the membrane potential, the Cl^- concentration gradient, and the $[Ca^{2+}]_i$ (Hartzell. et al., 2005). For example, if the Cl^- equilibrium potential (E_{Cl}) accompanied by the relatively high cytosolic Cl^- concentration in cells is more positive than the resting membrane potential, when $[Ca^{2+}]_i$ rises, the efflux of Cl^- leads to a depolarization of the plasma membrane and a series of more depolarization caused by the activation of voltage-gated Ca2+ channels (VGCCs) in

neuronal cells and water secretion in secretory cells. However, if E_{Cl} accompanied by the relatively low cytosolic Cl^- concentration is more negative than the resting membrane potential, opening CaCCs lead to hyper-polarization in neuronal cells, as $[Ca^{2+}]_i$ rising (Fig. 1).

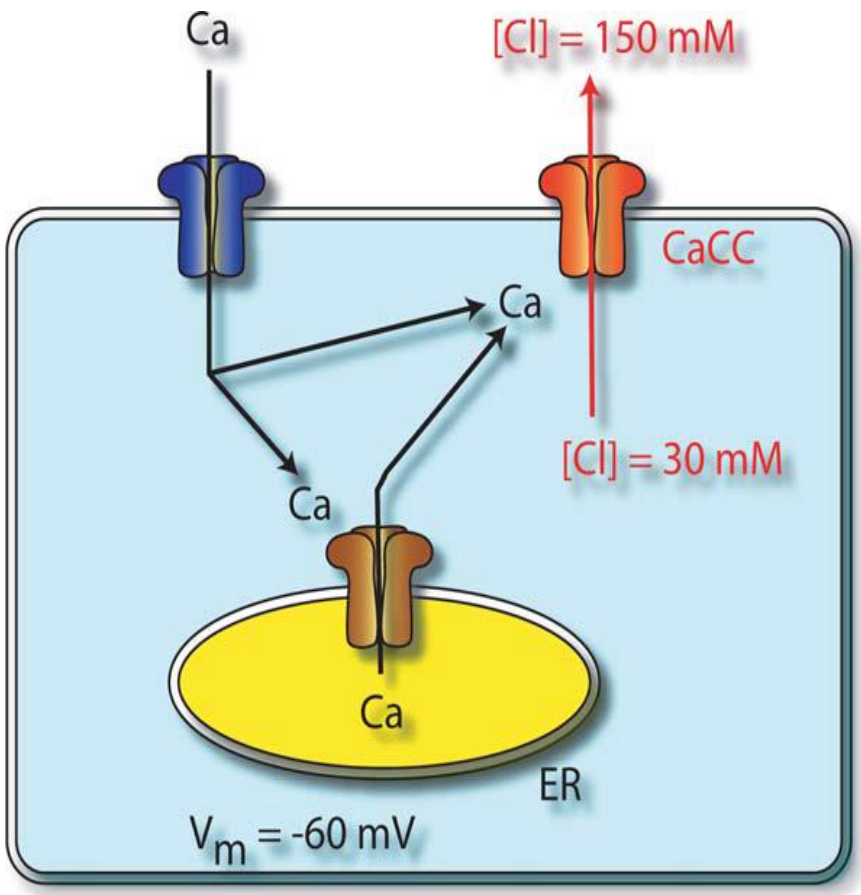

Figure 1. Factors controlling Cl^- flux through CaCCs.

Ca^{2+} influx through plasma membrane Ca^{2+} channels or release of Ca^{2+} from internal stores (ER) can stimulate CaCCs to open. Cl^- flux through open

CaCCs depends on the membrane potential and the Cl^- concentration gradient (Hartzell et al., 2005).

1.1.1 CaCCs in fluid Secretion

CaCCs are very important for fluid secretion by the airway, intestinal epithelium and exocrine glands (Kimelberg HK et al., 2000). The basic fluid secretion is accomplished by basally located transporters that accumulate Cl^- in the cell against the Cl^- electrochemical gradient and by the receptor-operated activation of apical Cl^- channels, such as CaCCs and cystic fibrosis transmembrane regulator (CFTR), which permit Cl^- to flow into the extracellular space down its electrochemical gradient (Boucher et al., 1989; Hartzell et al., 2005). In the airway epithelial cells, CaCCs are stimulated with ATP or UTP that stimulates Gq-coupled P2Y purinergic receptors to increase IP3 production and subsequently Ca^{2+} release. (Knowles et al., 1991; Tarran et al., 2002). The control of the airway mucous layer seems to be regulated by an interplay between CFTR and CaCCs (Tarran et al., 2002). Given that CFTR and CaCCs are both apical Cl^- channels, it has been proposed that the activatio-n of CaCCs could serve as a therapy for cystic fibrosis (Hartzell et al 2005). In the Intestinal epithelium, CaCCs can also secrete Cl^- transiently upon stimulation with carbachol, histamine, and nucleotides (Wasserman and Mukherjee, 1988; Dho et al., 1992; Kachintorn et al., 1993; Barrett and Keely, 2000) as like as the secretory mechanism of

the airway epithelial cells. In exocrine glands, Acinar and duct cells from lachrymal, parotid, submandibular, and sublingual glands secrete an isotonic, plasmalike primary fluid that is rich in NaCl and express CaCCs with similar properties above mentioned it (Melvin et al. 2005; Hartzell et al. 2005). The fluid secretion of these tissues is also Ca^{2+}-dependent and triggered by the parasympathetic neurotransmitter acetylcholine which binds to muscarinic receptor and subsequently drives the movement of Na^{+} through the parallel pathway and drags water, resulting in salty fluid secretion. (Douglas and Poisner, 1963; Botelho and Dartt, 1980; Hunter et al., 1983; Melvin et al., 1991). Thus CaCCs are central to the fluid secretion process because they constitute the last step in the transepithelial movement of Cl^{-}, which is the net driving force for the whole process (Hartzell et al., 2005) (Figure 2)

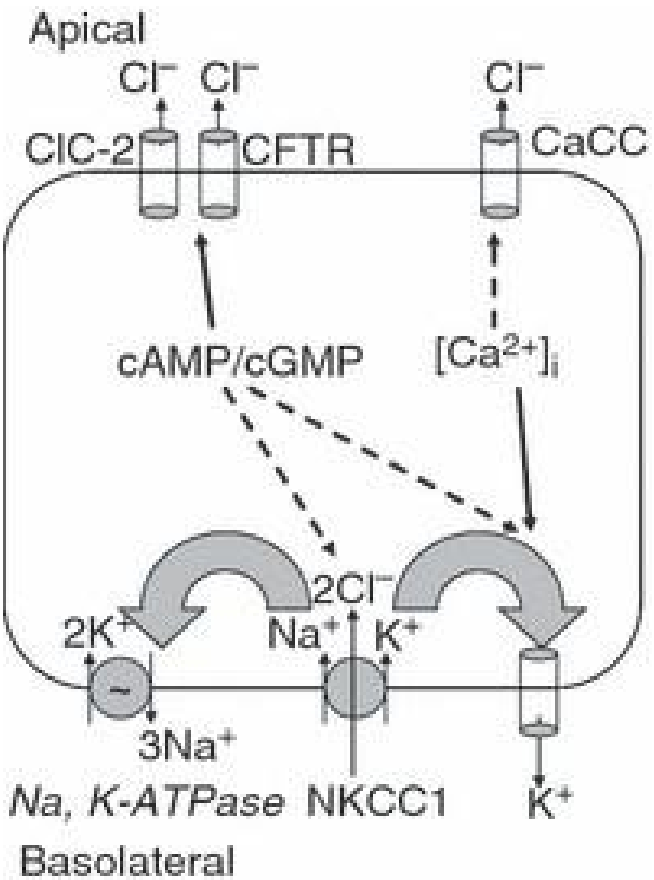

Figure 2. Model for fluid secretion in secretory epithelial cells

.

1.1.2. CaCCs in Smooth Muscle Contraction

CaCCs in smooth muscle are expected to produce membrane depolarization and sustain contraction, especially in response to excitatory agonists (Large and Wang, 1996; Saleh and Greenwood, 2005; Huang et al., 2012). The opening of CaCCs leads to depolarization of the membrane against the Cl^- electrochemical gradient in the cells, followed by opening of voltage-gated Ca2+ channels (VGCCs), and subsequent contraction. The CaCCs also open following the release of intracellular Ca2+ from internal stores such as sarcoplasmic reticulum store. The CaCC opening creates a spontaneous transient inward current (STIC), which can lead to increased contractility of rhythmically active smooth muscle cells (Bao et al.,2008).

1.1.3. CaCCs in Norvous System and Sensory Neuron

CaCCs are expressed in a variety of different neurons, including dorsal root ganglion (DRG) neurons, spinal cord neurons, and autonomic neurons. In most cases, CaCCs are not expressed in all neurons of a group, but rather in a subset, suggesting that these channels perform a specific function for this subset of neurons. The functions of CaCCs in neurons have been suggested that they are involved in action potential repolarization, generation of after-polarizations, and membrane oscillatory behavior. (Hartzell et al. 2005)

1.1.3.1. Role of CaCCs in Somatosensory neuron

The cell bodies of most somatosensory neurons are assembled in the dorsal root gauglia (DRG) from where they feed sensory signals into relay cells of the spinal cord, including information about skin temperature, touch, muscle tension, and pain because about 45–90% of them expresses CaCCs (Bader et al., 1987; Scott et al., 1988; Stapleton et al., 1994; Currie et al., 1995). In the mouse DRG, the CaCCs are expressed selectively in a subset of medium diameter (30–40 μm diameter) sensory neurons (Andre et al., 2003), suggesting that signaling in these neurons is somehow different from the rest of the population. This suggests that neurons express CaCCs to process sensory information in a tissue-specific manner. It has been proposed that CaCCs in DRG are responsible for after-depolarizations following action potentials (Mayer et al., 1985; De Castro et al., 1997). The estimated $[Cl^-]_i$ in DRG neurons is 30 mM (Kaneko et al., 2002), which produces an E_{Cl} of −35 mV. Thus opening CaCCs by Ca^{2+} entry or Ca^{2+} release from stores would depolarize the cell membrane or produce after-depolarizations (Crain, 1956; Deschenes et al., 1976; Duchen, 1990;). The CaCC current is upregulated in DRG neurons following axotomy (Sa´nchez-Vives and Gallego, 1994; Andre´ et al., 2003), suggesting that CaCCs have a role in neuropathic pain or nerve regeneration. In addition, in injured DRG neurons, the activity of Cl– channels generally results in further excitation

(Sung et al., 2000), which might enhance CaCC effects, leading to increased neuropathic pain.

1.1.3.2. Role of CaCCs in Olfactory receptor neuron

In vertebrates, a Ca^{2+}-activated Cl^- channel plays a central role in the transduction of odorous stimuli. When Odorants bind to and activate G protein– coupled receptors in the ciliary membrane of olfactory receptor neurons (Schild et al., 1998), these receptors activate adenylyl cyclase, which produces cAMP and turns on cyclic-nucleotide-gated channels that are permeable to both Na^+ and Ca^{2+}. This leads to a membrane depolarization and an elevation of $[Ca^{2+}]_i$ in the cilium, which activates CaCCs. The Cl^- efflux (inward current) depolarizes the membrane further. Thus, in olfactory receptor neurons, the Cl^- efflux through CaCCs serves as an amplification system of the odorant-activated current (Lowe G et al., 1993; Kleene, 1997). It has been estimated that the magnitude of *I*Cl.Ca can be as much as 30 times greater than the current through cyclic-nucleotide-gated channels (Reisert et al., 2003). Thus the physiologicalrole of the amplification could serve to increase the signal-to-noise ratio (Kleene, 1997) and hence to increase sensitivity to odorants. (Fig. 3)

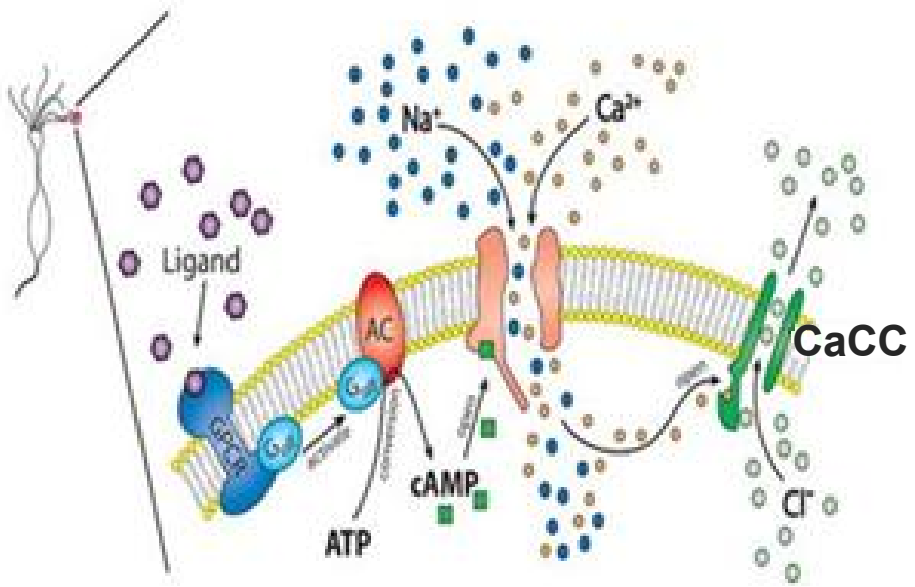

Figure 3. Model for sensory transduction in Olfactory receptor neuron through CaCC

1.2. Mechanisms of Activation and Regulation

There are two possible general mechanisms for Ca^{2+} to activate CaCCs: Ca^{2+} could bind directly to the channel protein or act indirectly on the channel via Ca^{2+}-binding proteins or Ca^{2+}-dependent enzymes. These two mechanisms seem to operate in different cell types, but may not be exclusive. (Hartzell et al. 2005)

1.2.1. Direct Activation by Ca^{2+}

CaCCs from salivary gland acinar cells (Martin, 1993), pulmonary endothelial cells (Nilius et al., 1997), ventricular myocytes (Collier et al., 1996), hepatocytes (Koumi et al., 1994), and glomerular mesangial cells (Ling et al., 1993) appear to be activated by direct Ca^{2+} binding to the channel protein. There are some evidences supporting direct gating of CaCCs by Ca^{2+}. In first, they activate both single channels and macroscopic currents even in the absence of any ATP required for phosphorylation (Kuruma et al., 2000). In seconds, they are also quickly activated by rapid application of Ca^{2+} to excised patches (Kuruma et al., 2000) or by photoreleasing Ca^{2+} in acinar cells isolated from pancreas and parotid glands (Park et al., 2001; Giovannucci et al., 2002). Further evidence in favor of the direct gating mechanism has been obtained when CaCC activation by increasing $[Ca^{2+}]_i$ with ionomycin was not prevented by preexposure of cells

to KN-62 or peptide inhibitors of calmodulin and of CaMKII (Arreola et al. 1998). In addition the apparent affinity of CaCCs for Ca^{2+} is in the micro-molar range and Ca^{2+} binding to CaCCs from different tissues is voltage sensitive. At high positive membrane potentials Ca2+ appears to bind better to the channel protein than at low negative potentials (Arreola et al. 1996; Kuruma et al., 2000; Reisert et al., 2003).

1.2.2. Activation by Phosphorylation via CaMKⅡ

Some CaCCs from the human colonic tumor cell line T84 (Worrell et al., 1991; Chan etl al., 1994; Kaetzel et al., 1994; Xie et al., 1996; Xie et al., 1998), airway epithelia (Wagner et al., 1991), T lymphocytes (Nishimoto et al., 1991), human macrophages (Holevinsky et al., 1994), biliary epithelial cells (Schlenker T and Fitz JG, 1996), and cystic fibrosis-derived pancreatic epithelial cells (Chao et al., 1995) are also stimulated by protein phosphorylation involving the calmodulin-independent protein kinase CaMKII. Evidence supporting the participation of CaMKII in CaCC activation has been provided by the use of inhibitors of calmodulin or CaMKII or by cell dialysis with the purified enzyme in a variety of cells including colonic T84, airway epithelia, and neutrophils (Wagner et al., 1991; Worrell et al., 1991; Nishimoto et al., 1991). In contrast, dialysis of the purified enzyme into airway epithelial cells and neutrophils activates chloride currents (Wagner et al., 1991; Nishimoto et al., 1991).

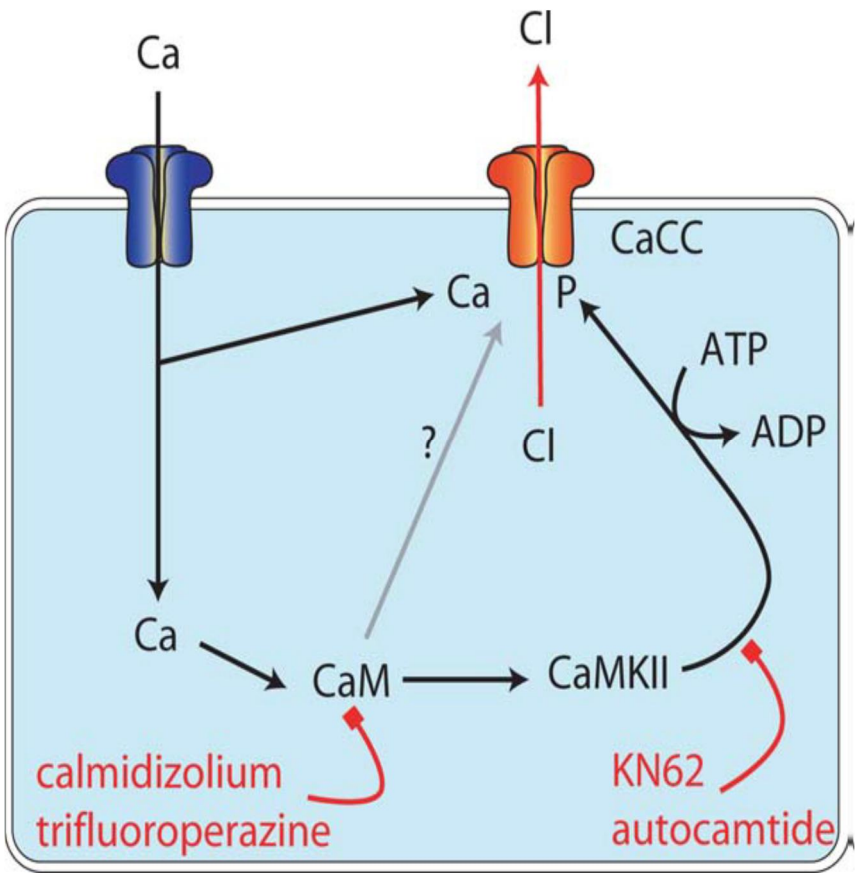

Figure 4. Pathways regulating CaCCs.

Ca^{2+} influx or release from stores can stimulate CaCCs either directly of via calmodulin (CaM) -dependent pathways, including phosphorylation via CaMKII. Blockers are shown in red. (Hartzell et al. 2005)

1. 2.3. cGMP-dependent Activation

In artery smooth muscle cells, the cGMP-dependent CaCCs which absolutely requires cGMP exist (Piper and Large, 2003; Matchkov et al.,

2004) and is potentiated by CaM but unaffected by CaMKII blockade (Piper and Large, 2004).

1.2.4. pH-dependent Inhibition

A decrease in intracellular pH inhibits CaCCs in acinar cells from lachrymal and parotid glands as well as from T84 cells (Par and Brown, 1995; Arreola et al., 1995). The physiological relevance of CaCC regulation by H^+ is also not clear. It may serve as a negative feedback loop for the exit of $HCO3^-$ through CaCC and thereby prevent excessive cytosolic acidification of the cell (Begenisich and Melvin, 1998).

1.3. Activation kinetics of CaCC

The activation kinetics of CaCCs by increasing $[Ca^{2+}]_i$ has been studied by applying constant amounts of Ca^{2+}, by photoreleasing Ca^{2+}, by inducing Ca^{2+} release from intracellular pools by IP3, or by enhancing Ca^{2+} entry by application of Ca^{2+} ionophores (Evans and Marty, 1986; Okada et al., 1995; Arreola et al., 1996; Hartzell, 1996; Nillius et al., 1997a; Kuruma and Hartzell, 2000; Giovannucci et al., 2002). When $[Ca^{2+}]_i$ is below ~1 μM, $I_{Cl.Ca}$ is both voltage and time dependent, but at higher $[Ca^{2+}]_i$, the voltage and time dependence disappears. Also, at $[Ca^{2+}]_i$ less than ~1 μM, CaCCs activate slowly reaching a steady state in ~2 s. The resulting activation time constants appear voltage independent at constant $[Ca^{2+}]_i$. However, as

$[Ca^{2+}]_i$ increases, the activation rate is accelerated. In contrast, the deactivation of CaCCs follows a time course that is described by a single exponential, with a time constant that is voltage dependent. The resulting current-voltage relationship shows outward rectification at low $[Ca^{2+}]_i$ (< 500 nM). This rectification is nearly lost by rising $[Ca^{2+}]_i$ to >1 μM (Evans and Marty, 1986; Arreola et al., 1996; Kuruma and Hartzell, 2000). The apparent open probability (P_o) of CaCCs is voltage dependent. As $[Ca^{2+}]_i$ is increased, the activation curve is shifted toward more negative voltages. From the analysis of the $[Ca^{2+}]_i$ dependence of P_o, it is estimated that more than one Ca^{2+} ion is needed to activate one channel. Hill coefficients of 2 to 5 have been estimated from dose-response curves, thus suggesting the presence of multiple Ca^{2+}-binding sites in the channel protein (Arreola et al., 1996; Kuruma and Hartzell, 2000). The outward rectification that is seen at low $[Ca^{2+}]_i$ may be explained by the fact that the apparent affinity of CaCCs for Ca^{2+} is voltage dependent (Arreola et al., 1996; Nillius et al., 1997a; Kuruma and Hartzell). This implies that positive voltages induce rearrangements of the Ca^{2+}-binding sites to favor interaction with Ca^{2+} ions to increase P_o. (Hartzell et al. 2005)

1.4. Molecular Identity of CaCCs

Clearly, elucidating the molecular identity of CaCCs is an important for understanding the role of these channels in normal physiology, as well as

in disease. At present, three or possibly four molecular candidates have been proposed to be CaCCs.

1.4.1. CLCA

This protein had no resemblance with other known ion channels. Various paralogs and orthologs of CLCA were subsequently identified in various species, including human and mouse. However, the membrane currents elicited by expression of CLCA proteins did not resemble the "canonical" CaCCs in terms of voltage-dependence, Ca^{2+} affinity, and sensitivity to pharmacological modulators (Jentsch et al. 2002; Eggermont, 2004; Hartzell et al., 2005). There is a general consensus now that CLCAs are not channel forming proteins but rather cell adhesion molecules (CAM) which may be also released as soluble proteins in the extracellular medium (Patel et al., 2009; Ferrera et al., 2011).

1.4.2. ClC-3

ClC-3 is a member of the ClC channel family. It was found that expression of ClC-3 is associated with the appearance of voltage-independent Cl^- currents whose activation requires phosphorylation by the CaMKII (Huang et al., 2001). These findings contrast with the notion of ClC-3 being a H^+/Cl^- transporter of intracellular organelles (Matsuda et al. 2010). Furthermore, salivary gland cells of ClC-3 knockout mice have

normal CaCC activity (Arreola et al., 2002). Such findings rule out the direct involvement of ClC-3 in forming the classical CaCCs but allow the possibility that ClC-3 contributes to the expression/activity of a Cl− channel that is specifically regulated by CaMKII. (Ferrera et al., 2011)

1.4.3. Bestrophin 1

Bestrophin 1, the product of the *VMD2* gene that is highly expressed in the retinal pigment epithelium, is the protein mutated in Best vitelliform macular dystrophy, a disease characterized by macular degeneration and blindness (Petrukhin et al., 1998). Expression of bestrophins in heterologous expression systems elicited the appearance of Ca^{2+}-activated Cl^- currents whose activity is altered by site-directed mutagenesis (Qu et al., 2004). Nevertheless, there are other findings indicating that bestrophins are a type of Cl^- channel different from CaCCs and also involved in the regulation of other functions (Ferrera et al., 2011). In particular, the bestrophin-dependent membrane currents show some differences with respect to the CaCCs described in many cell types, particularly regarding the small dependence of gating on membrane potential (Hartzell et al., 2008; Qu et al., 2004). Furthermore, mice with genetic ablation of bestrophin-1 have normal Ca^{2+}-activated Cl^- currents in cells from the retinal pigment epithelium (Marmorstein et al., 2006). Recently, bestrophin-1 has been also proposed as a Cl^- channel of the endoplasmic reticulum (Barro-Soria et al., 2010). In

this location, bestrophin dependent Cl^- transport would be important to dissipate the electrical potential difference that otherwise is generated at the ER membrane by Ca^{2+} fluxes (Ferrera et al., 2011). Indeed, bestrophin-1 expression influences the release of Ca^{2+} release from the ER and, consequently, the activation of Ca^{2+}-dependent K^+ and Cl^- channels in the plasma membrane (Barro-Soria et al., 2010).

1.4.4. Anoctamin 1/TMEM16A

TMEM16A belongs to the family of "Transmembrane proteins with unknown function 16," abbreviated as TMEM16, which includes nine other family members (Ferrera et al., 2011). TMEM16A is also known as anoctamin 1 (abbreviated ANO1), nomenclature that incorporates the concepts that TMEM16 family members are anion channels and have eight putative transmembrane segments (Yang et al., 2008). In 2008, three research groups identified ANO1 as a CaCC-forming protein (Caputo et al., 2008; Schroeder et al., 2008; Yang et al., 2008). These laboratories took different approaches but all reported the same molecule, ANO1, as a bona fide CaCC. Using the independent and different approaches, Caputo and colleagues recognized that CaCCs are up-regulated in interleukin-4-treated human bronchial epithelial cells and identified ANO1 from a microarray of global gene expression analysis and siRNA gene-silencing experiments (Caputo et al., 2008). Yang and colleagues pinned down ANO1 from a

bioinformatic screen for novel membrane proteins with more than two transmembrane domains (Yang et al., 2008). Schroeder and colleagues used instead an expression cloning approach. They started from the observation that Axolotl oocytes, in contrast to Xenopus oocytes, do not have endogenous expression of CaCCs. Therefore, Axolotol oocytes were used for the screening of cDNA libraries which detected Xenopus ANO1 as the clone generating CaCC-like currents (Schroeder et al., 2008). In all three studies, heterologous expression of ANO1 in different cell types also generated Cl^- currents with the classic properties of CaCCs. Furthermore, ANO1 has been appeared as an important component of the CaCC according to several independent lines of evidence. First, expression of ANO1 in various expression systems generates Cl^- currents with characteristics very similar to those of CaCCs, including voltage dependence, affinity for Ca^{2+}, ion selectivity, and pharmacological sensitivity (Caputo et al., 2008; Schroeder et al., 2008; Yang et al., 2008). Second, silencing of ANO1 by RNA_i causes significant inhibition of CaCCs in all cells tested so far. Finally, ANO1 knockout mice have significantly reduced Ca^{2+}-dependent Cl^- transport in different organs (Ousingsawat et al., 2009; Rock et al., 2009; Romanenko et al., 2010).

2. Expression and physiological function of ANO1

With ANO1 as a newly discovered CaCC, it is now trying to answer the following questions: Is the TMEM16 family responsible for the endogenous CaCC? How do they contribute to physiological processes? (Huang et al., 2012) The knockout mouse for ANO1 was generated after the observation of ANO1 enrichment in the zone of polarizing activity at the distal limb, before molecular identification of ANO1 as CaCC (Rock et al., 2008). These mice have been used to validate ANO1 expression and function by immunecytochemistry, biophysical and physiological studies (Flores et al., 2009; Galietta, 2009; Gomez-Pinilla et al., 2009; Gritli-Linde et al., 2009; Huang et al., 2009; Hwang et al., 2009; Rock et al., 2009).

2.1. Fluide secretion

ANO1 knockout mice exhibit significant neonatal lumenal mucus accumulation in the trachea, which could result from insufficient fluid secretion for mucus hydration. Developmental defects resulting in tracheomalacia could also impair mucus clearance (Rock et al., 2009). In addition, studies with knockout mice or RNA silencing technology have demonstrated that ANO1 constitutes the native CaCCs in many cells, including epithelial cells in the salivary gland, pancreatic gland, airway, and gastrointestinal tract (Almaca et al., 2009; Huang et al., 2012b; Rock et al.,

2009; Yang et al., 2008), and interstitial cells of Cajal (Huang et al., 2009; Hwang et al., 2009). Its expression has also been found in the porcine bronchial submucosal gland serous acinar cells, which may mediate the agonist-induced fluid secretion in those cells (Lee and Foskett, 2010).

2.2. Muscle contraction

Reduction of ANO1 expression with siRNAs in pulmonary artery smooth muscle cells led to an almost total loss of whole-cell CaCC currents (Manoury et al., 2010). TMEM16A mRNA is also detected in smooth muscle cells isolated from mouse portal vein, thoracic aorta, and carotid artery with varied abundance (Davis et al., 2010). Further studies incorporating negative controls such as knockout mice or RNA interference knockdown have demonstrated that TMEM16A constitutes the native CaCCs in airway and vascular smooth muscle cells (Huang et al., 2012b; Manoury et al., 2010; Thomas-Gatewood et al., 2011; Wang et al., 2012). Also, tracheomalacia in TMEM16A knockout mice could result from the abnormalities of smooth muscle activity during airway development. It will be interesting to investigate whether ANO1 is responsible for STICs and how ANO1 regulates the contraction of smooth muscle cells (Ma et al., 2016).

2.3. Nociception

In investigating the mechanisms involved in acute nociceptive signaling in small DRG neurons, Liu and colleagues found that bradykinin-activated CaCC currents were mediated by ANO1 (Liu et al. 2010). In addition Cho and colleagues found that ANO1 is a heat sensor that detects nociceptive thermal stimuli in sensory neurons and possibly mediates nociception (Cho et al., 2012). These results are in agreement with previous report, where TMEM16A was found highly expressed in the majority of small DRG neurons. (Yang et al. 2008)

2.4. Benign prostatic hyperplasia (BPH)

ANO1 was highly amplified in dihydrotestosterone (DHT) treated prostate epithelial cells, whereas the selective knock down of ANO1 inhibited DHT-induced cell proliferation. Therefore, ANO1 is essential for the development of prostate hyperplasia and is a potential target for the treatment of BPH (Cha et al., 2015).

3. Structure and function of ANO1

3.1. Topology

The topology of ANO1 has been investigated by many researchers.

First, Hydropathy analysis predicted that all members of the ANO family have eight transmembrane domains with cytosolic N- and C- termini. Das and colleagues predicted a re-entrant loop between transmembrane domains 5 and 6 using inserted hemagglutinin-tag accessibility (Das et al., 2008). This re-entrant loop has been proposed to form the pore of ANO1 because of the altered relative anion:cation selectivity of mutations in this region (Yang et al., 2008). However, a revised model of ANO1 topology has been proposed based on mutagenesis, epitope accessibility and cysteine-scanning accessibility (Yu et al., 2012). In this revised model, the reentry loop is intracellular and contains two acidic amino acids E702 and E705, which contribute to Ca^{2+} gating of the channel (Yu et al., 2012).

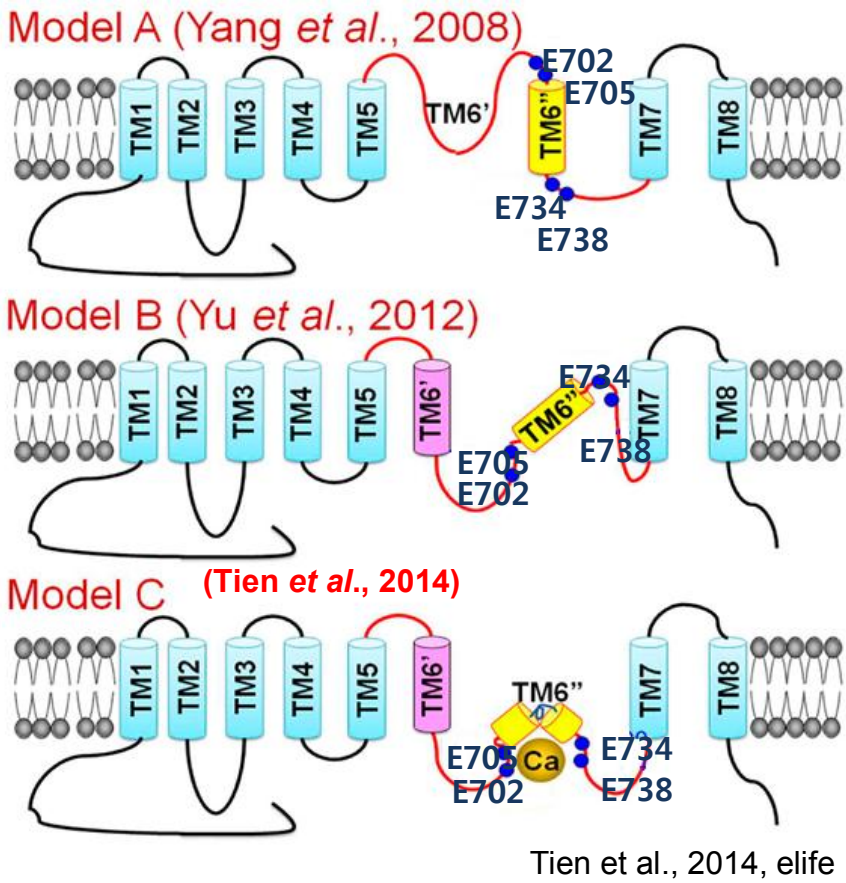

Figure 5. The predicted topologies of ANO1

The figure shows two different topologies proposed for ANO1 protein. In the model A (top), the region between transmembrane domains 5 and 6 constitutes a reentrant loop that faces the extracellular environment and is important for the formation of the ion pore. In the model B (middle), this region crosses completely the membrane (forming the sixth transmembrane domain) and then generates a cytosolic loop important for Ca^{2+} binding. In the model C (bottom), it represent the new position of the putative calcium binding residues (E702, E705, E734 and D738) based on two previous membrane topological models (Model A and B) (Tien et al., 2014).

3.2. Stoichiometry

Several studies have demonstrated that the quaternary structure of TMEM16A channels as homodimers using biochemical methods such as native polyacrylamide gel electrophoresis, Forster resonance energy transfer, and co-immunoprecipitation (Fallah et al., 2011; Sheridan et al., 2011; Tien et al., 2013). The dimerization of TMEM16A subunits occurs intracellularly before the channel is trafficked to the plasma membrane (Sheridan et al., 2011). Also, the cytosolic N-terminus of TMEM16 A is necessary and sufficient for channel dimerization (Tien et al., 2013). The association of TMEM16A subunits is likely due to noncovalent protein-protein interactions mediated via a predicted helical segment (residues 161-179) in the N-terminus of TMEM16A (Tien et al., 2013). It has been reported that TMEM16A subunits can heterodimerize with TMEM16B subunits, but not TMEM16F subunits (Tien et al., 2013), further suggesting that TMEM16A and TMEM16F are different in dimeric organization. Since mutations in the dimerization domain greatly reduced TMEM16A currents (Tien et al., 2013), TMEM16A without the dimerization domain is expected to be a nonfunctional channel (Ma et al. 2016).

3.3. Ca^{2+} and Voltage sensing of ANO1

At low concentrations of Ca^{2+}, ANO1 currents are activated by depolarization and deactivated by hyperpolarization. Conversely, membrane depolarization increases Ca^{2+} sensitivity of ANO1 channel (Xiao et al., 2011). Since a Ca^{2+}-binding site is thought to be within the electric field of the membrane (Brunner et al., 2014), the voltage-dependent gating of ANO1 in the presence of Ca^{2+} may be explained by facilitation of Ca^{2+} binding to its binding site upon membrane depolarization. In addition, even in the absence of Ca^{2+}, ANO1 can be activated by strong depolarization (+200 mV), suggesting that ANO1 exhibits voltage-dependent activation mechanism which is independent of Ca^{2+} (Xiao et al., 2011). Furthermore, the voltage-dependent feature is confirmed in purified TMEM16A proteins (Terashima et al., 2013), suggesting that TMEM16A has an intrinsic voltage sensor independent of other associated proteins. The voltage-dependent current was significantly increased in ANO1 channels lacking the EAVK exon (splice variance c), and decreased in ANO1 channels with the mutation of the 444EEEE447 residues in the first intracellular loop (Xiao et al., 2011). Also, the six acidic amino acids (E444A, E445A, E446A, E447A, E448A, and E457A) in the first intracellular loop contributed to voltage-dependence of ANO1 (Xiao and Cui, 2014). However, these acidic residues in the intracellular loop are unlikely to directly sense the transmembrane voltage

change because the hydrophilic intracellular loop is not located within the transmembrane voltage field. Unlike the voltage-sensitive ion channels, ANO1 does not contain a classic voltage-sensing domain in voltage-gated ion channels. The equivalent gating charge of ANO1 is approximately 0.33, which is about 4-6 fold less than that of voltage-gated ion channels (Xiao and Cui, 2014; Xiao et al., 2011), suggesting that the voltage sensor in TMEM6A channels is likely different from that in voltage-gated ion channels.

In addition, the permeated anions are known to affect voltage-dependent gating of ANO1 (Cruz-Rangel et al., 2015; Xiao et al., 2011). It is assumed that anion occupancy of the pore stabilize the open state, and thereby contributes to channel gating (Xiao et al., 2011). This hypothesis is supported by recent findings, showing that extracellular Cl^- regulates ANO1 by stabilizing the open state and contributing to voltage-dependent activation of TMEM16A (Contreras-Vite et al., 2016).

4. Other ANO Family

There are a total of 10 members in the vertebrate ANO family. Sequence similarity and phylogenetic analysis shows that ANO2 shares the highest sequence homology with ANO1, with 56.5% sequence identity and 71.4% similarity. ANO3 and ANO4 share 58.9% sequence identity and 72.2%

similarity. ANO5 and ANO6 are 46.8% identical and 64.6% similar. ANO8 and ANO10 might constitute a subfamily of TMEM16 proteins, because they are genetically distant from the other eight members of the family in the phylogenetic tree (Figure 6).

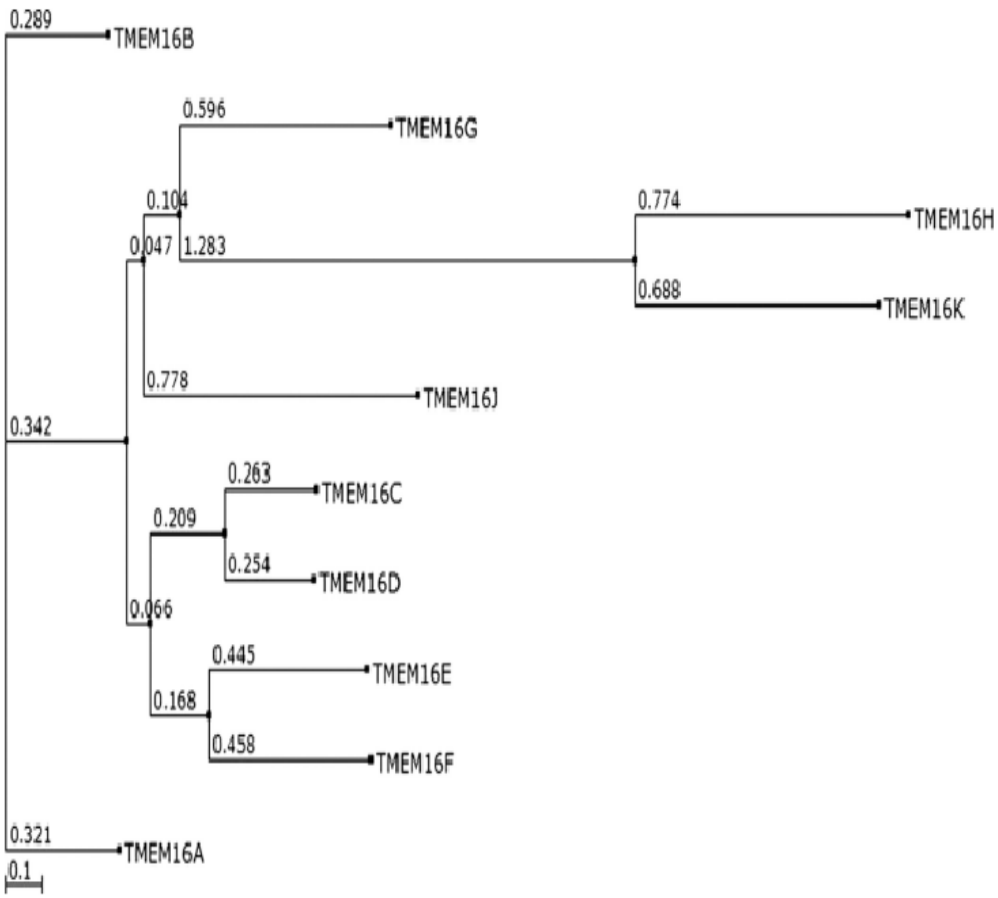

Figure 6. Phylogenetic analysis of 10 members of mouse ANOs proteins. (Huang et al. 2012)

4.1. Anocatmin 2/TMEM16B (ANO2)

ANO2 is the only member so far that has been shown to function as a CaCC in heterologous expression systems, and it may account for the endogenous CaCC in olfactory cilia and retinal synapses (Schroeder et al., 2008; Pifferi et al., 2009; Sto¨hr et al., 2009; Rasche et al., 2010; Sagheddu et al., 2010). In previous report, the disruption of the ANO2 in mice abolished Ca2+-activated Cl- currents in OSNs but did not produce any major change in olfactory behavior (Billig et al., 2011). However, recently, TMEM16B knockout (KO) mice have behavioral deficits in odor-guided food-finding ability (Pietra et al., 2016). ANO2 is also expressed in retinal synapses and brain (Sto¨hr et al., 2009), When expressed in HEK-293 cells, ANO2 channels generated Cl_ currents very similar to those of native CaCCs previously described in photoreceptors. Subcellular localization and functional properties suggested that TMEM16B is a main CaCC forming protein of photoreceptors (Sto¨hr et al., 2009). In addition, a recent study has revealed that ANO2 is implicated in an inhibitory effect on neuronal excitability, such as controlling action potential firing and frequency in the somatodendritic region of hippocampal neurons (Huang et al., 2012). In biophysical properties, ANO2 channels have lower Ca^{2+} sensitivity than that of ANO1 and faster kinetics of activation and deactivation following membrane depolarization and hyperpolarization, respectively. The relatively

low Ca^{2+} sensitivity of ANO2 is consistent with that of olfactory Cl^- channels (Kleene and Gesteland, 1991; Hallani et al., 1998). This characteristic may be evolved to adapt to the high local Ca^{2+} concentrations reached in the small volume of olfactory cilia during stimulus. (Ferrera et al., 2011)

4.2. Anocatmin 6/TMEM16F (ANO6)

ANO6, robustly expressed on the surface of many different cell types (Schreiber et al., 2010) was found recently to affect the phospholipid scramblase activity in platelets (Suzuki et al., 2010). Interestingly, ANO6 is endowed with Cl- channel activity although the biophysical properties of TMEM16F-dependent channels differ among studies, such as a component of the outwardly rectifying Cl^- channel (Martins et al. 2011) and Ca^{2+}-activated Cl- channels (Grubb et al., 2013; Shimizu et al., 2013). Furthermore, ANO6 is also identified as a nonselective cation channel (Yang et al. 2012). The platelets, erythrocytes, and B-cells from ANO6 knockout mouse showed reduced Ca^{2+}-dependent PS exposure, in agreement with the function of TMEM16F as a scramblase component. Importantly, $ANO6^{-/-}$ mice showed impaired coagulation, as measured by thrombin generation, and prolonged bleeding, thus resembling the phenotype of Scott syndrome patients. The knockout animals were also

markedly less prone to induced carotid artery thrombosis compared with wild-type mice. (Yang et al. 2012; Pedemonte and Galietta, 2014)

4.3. Other Anocatmin/TMEM16 (ANO) Family

TMEM16C/ANO3 facilitates Na^+-activated K^+ currents in rat sensory neurons and regulates pain processing despite no function as channel by itself in a heterologous expression system (Huang et al., 2013). Also ANO3 expression elicited scrambling of PC and GalCer but not of PS. TMEM16D/ANO4, TMEM16F/ANO6, TMEM16G/ANO7, and TMEM16J/ANO9 mediate Ca^{2+}-dependent scrambling of phosphatidylserine (PS), phosphatidylcholine (PC), and galactosylceramide (GalCer). Interestingly, ANO4-expressing cells showed a significant level of scramblase activity under resting conditions, in the absence of intracellular Ca^{2+} elevation (Suzuki et al., 2013). Some ANOs, namely, ANO5, ANO8, and ANO10, had neither scramblase nor channel activity due to a prevalent intracellular localization of these proteins. In addition, some ANOs form heterooligomers. For example, coexpression of ANO1and ANO9 elicited a level of anion transport activity that was smaller than that elicited by ANO1 alone (Schreiber et al., 2010). This inhibition may arise from a direct interaction between the two types of proteins. Such a possibility indicates that the results obtained from heterologous expression of ANO1 in some null systems such as HEK-293 or FRT cells may be

significantly affected by the endogenous expression of other ANOs, particularly ANO6, ANO8, and ANO10 (Schreiber et al., 2010).

Aim of this study

Since ANO1 was identified as Ca^{2+}- activated chloride channel (CaCC), a variety of studies have been implemented to identify their physiological roles, such as epithelial secretion, smooth muscle contraction, cardiac excitability and nociception. ANO2 has also turned out the CaCC implicated in the regulation of membrane excitability in neurons and olfaction in ORNs (Billig et al., 2011; Huang et al., 2012; Pietra et al., 2016). Moreover, ANO6 has been revealed as both the CaCC and scramblase which is Ca^{2+}-dependent Phospholipid scrambling (PLS), implicated in Scott Syndrome, a blood clotting disorder where platelets fail to expose phosphatidylserine (PS) in response to cytosolic Ca^{2+} increase (Suzuki et al., 2010; Yang et al., 2012; Kmit et al., 2013).

With the importance for physiological roles of the Anoctamin family, understanding its structure and activation mechanism by Ca^{2+} has also emerged as a key issue in Anoctamin studies. Despite many researches to find Ca^{2+} binding site of ANO1, however it has been difficult to identify Ca^{2+} binding site because of several limits, such as the absence of the exact knowledge for topology, the absence of any Ca^{2+} binding motifs such as EF-hand, IQ-motif within its amino acid sequence and discrepancy of the measured Ca^{2+} sensitivity according to the different methods for patch clamp recording or making solution including free Ca^{2+}.

Thus, in this study, we introduced some impressive attempts such as homology modeling, surface plasmon resonance and quantitative analysis of a variety of Ca^{2+} concentrations to find a specific Ca^{2+} binding region of ANO1 and to predict a mechanism by which ANO1 is activated by cytosolic Ca^{2+}.

Methods

1. Mutagenesis and gene expression

All mutants were generated from the wild-type construct of mouse ANO1 a, c splice variant (pEGFP-N1-mANO1). Amino acid substitution or deletion mutants were prepared using a site-directed mutagenesis kit (Muta-direct, iNtRON Biotech) or by using the overlap PCR method. Mutations in all mutants were confirmed by sequencing whole nucleotide sequences. HEK293T cells were transfected with mixture which consist of 1μg of pEGFP-N1-mANO1 or pEGFP-N1-mutants using fuGENE (Roche Diagnostics, Penzberg, Germany) in 35-mm dishes and cultivated in DMEM supplemented with 10% fetal bovine serum (GIBCO) and Penicillin-streptomycin at 37℃ in a 5% CO^2 incubator. Cells were used 1 or 2 days after transfection.

2. Electrophysiology

Borasilicate glass pipettes (World Precision Instrument, Sarasota, FL) with tip resistances of ~2MOhms were prepared from micropipette puller (Sutter Instrument, Novato, CA) and used to form gigaseals on HEK293T cells. The two recording methods for patch clamp were used. For whole cell recording, the cell were ruptured through a few gentle suction once the state of gigaseal were made on cell attached with pipette. Inside-out membrane pathes were excised by pulling the pipette away from the cell. Currents were recorded with a patch-clamp amplifier (Axopatch 200B, Molecular Probes) with a 1-KHz filter. Data from the amplifier were digitized with Digidata 1440A (Molecular devices) and stored on a computer.

The both control pipette solution and bath solution for whole cell recording were identified as using same solutions contained 140 mM N-methyl D-glucamine, 2 mM $MgCl_2$, 10mM HEPES adjusted at pH 7.2. The control pipette solution for inside-out patch recording contained 140 mM N-Methyl D-glucamine, 2 mM $MgCl_2$, and 10 mM HEPES adjusted to pH 7.2. For Ca^{2+}-free solution, 10mM ethylene glycol tetraacetic acid (EGTA) was added to the control solution. The bath solution for inside-out patch recording contained (in mM) 140 N-methyl D-glucamine, 2 $MgCl_2$, 10 HEPES, 10 chlelator (EGTA, N(2hydroxylethyl) ethylenediamine triacetic acid (HEDTA), or nitrilotriacetic acid (NTA)), and a calculated amount of

$CaCl_2$ (adjusted with HCl to pH 7.2). EGTA was used for 0.1 ~ 1.0 μM free Ca^{2+}, whereas HEDTA and NTA were used for 3.0 ~ 30 and 100 ~ 1,000 μM free Ca^{2+}, respectively (Tsunenari T et al., 2005). No chelator was added to solutions with free Ca^{2+} greater than 1 mM. To calculate free Ca^{2+} in solution, the WEBMAXC program was used (http://www.stanford.edu/~cpatton/webmaxc/webmaxcS.htm). To confirm free Ca^{2+} less than 30 μM in each solution, the solutions was monitored with Fura-2 fluorometry (Jung J et al., 2013).

3. Surface plasmon resonance measurement

A Biacore3000 was used for kinetic surface plasmon resonance measurement as previously described (Hyun S et al., 2011). Briefly, a biotinylated peptide (692-NLEPFAGLTPEYMEM-706) was immobilized on a SA chip or custom streptavidin-coated CM5 sensor chip (GE Healthcare), with one flow with biotin alone as a reference cell. For the binding assay, HEPES-buffered saline containing 0.005% of Tween 20 was used as a running buffer. Various concentrations of the reference helix peptide (aa 651-671) were injected for 120s and dissociated for 240s at a flow rate of 20 μL/min. Binding curves were analyzed using BIAevaluation 3.1.

4. Structure homology modeling

The amino acid residues of the third intracellular loop (residues 603-663) in ANO2 were selected as the target sequence for homology modeling. Automated homology modeling was implemented by MODWEB (http://salilab.org/modweb), a web server for automated comparative protein structure modeling.

5. Data analysis

Data analysis was performed with Clampfit 10 (Molecular Devices). Dose response relationships were fit to the Hill equation of the form:

$$\frac{I}{Imax} = \frac{1}{\left(1 + \frac{[Ca2+]}{EC50}\right)^{n}}$$

Where I is current, $[Ca^{2+}]$ is Ca^{2+} concentration. Imax is the maximum current evoked by the highest $[Ca^{2+}]$ treated into each patches. EC_{50} is the half-maximal concentration of Ca^{2+}. n is the Hill coefficient which is indicative of the cooperativity of Ca2+ binding.

To estimate the voltage dependence, the magnitude of tail currents (I_{tail}) was measured at 100-200 μs after each voltage pulses of repolarization at -100mV to calculate the tail conductance (G_{tail}). Using the above equation, G_{tail} was converted from the magnitude of I_{tail} at each V_m:

$$\mathrm{Gtail} = \frac{\mathrm{Itail}}{\mathrm{Vm} - \mathrm{Vrev}}$$

For G/G_{max} vs V_m curve, the data was fitted to the Boltzmann equation:

$$\frac{\mathrm{G}}{\mathrm{Gmax}} = \frac{1}{1 + \mathrm{e}^{(\mathrm{Vm} - \mathrm{V1/2})\frac{\mathrm{zF}}{\mathrm{RT}}}}$$

Normalization was performed using G_{max} to obtain G/G_{max}, which is proportional to the apparent open probability of the channel. Z is the equivalent gating charge associated with voltage-dependent channel opening. V1/2 is the halfmaximal membrane potential related to the conformational energy associated with voltage-independent channel opening. F/RT = 0.039 mV^{-1}.

Results

1. The third intracellular loop essential for ANO1 activation by Ca^{2+}

1.1. Ca^{2+}-activated anoctamin family

ANO1 belongs to a protein family consisting of ten members ANO1-10 with a high degree of structural similarity. (Tian et al., 2012) Although ANO1 and ANO2 were revealed as Ca^{2+} activated chloride channel (CaCC), it is still controversial whether their other members ANO3-ANO10 are also CaCC or not. (Tian et al., 2012, Duran et al., 2012) Based on the idea through which Ca^{2+} activated anoctamin family might have a conserved Ca^{2+}- binding site, first of all, we checked the intracellular localization of anoctamin family from HEK293T cell transfected by the ANO genes tagged on the C-terminus with enhanced green fluorescence protein (EGFP) (Figure 7) and measured the Ca^{2+} sensitivity of ANO family to distinguish the ability to be activated by Ca^{2+} (Figure 8). Among splice variants of ANO1, we used an a,c-splice variant that has 116 residues in the N-terminus and the 448-EAVK-451 insert. (Galietta et al., 2009) For inside-out patch recording, at + 80mV holding potential (E_h), ANO1 was activated by Ca^{2+} with a half-maximal concentration (EC_{50}) of 0.9 μM. ANO2 displayed EC_{50} of 9.8 μM.

However, ANO3 and ANO6-9 appeared to be less sensitive to Ca^{2+} than those of ANO1 and ANO2 at +80 mV, with EC_{50} of 32.2, 50.7, 935, 29 and 25 μM, respectively (Figure 8a, b). Also, at – 80 mV, ANO1 and ANO2 are less sensitive to Ca^{2+} than those at +80 mV, with respective EC_{50} values of 2.77 and 14.33 μM. ANO3, 6-9 failed to respond to Ca^{2+} at -80mV (Figure 9a., b). Moreover, ANO1 and ANO2 were progressively activated when the membrane potential was made more positive. The resulting current-voltage relationship of ANO1 and ANO2 showed outward rectification at low $[Ca^{2+}]_i$ and non-rectification at high $[Ca^{2+}]_i$, which is the specific characteristic of the classic CaCC (Hartzell et al., 2005) (Figure 9a, b). However, other ANO channels showed outward rectification at every concentration of $[Ca^{2+}]_i$ (Figure9c, d). In addition, Subdued (CG16718) is an ortholog of mammalian TMEM16A and B from *Drosophila melanogaster* shows 32.8% identity with mouse ANO1. We confirmed that it was also activated by Ca^{2+} when it was transfected into HEK293T cells as previously reported with EC_{50} of 31.5 μM at +80 mV showing current-voltage relationship of outward-rectification pattern at every concentration of Ca^{2+} (Figure 10). (Xiu Ming Wong et al., 2014; Wijeong Jang et al., 2015)

Thus, these results indicate that the ANO1 and ANO2 only have the high Ca^{2+} sensitivity to both negative and positive E_h which are specific characteristic of the classic CaCC although other ANO channels are activated by the Ca^{2+}.

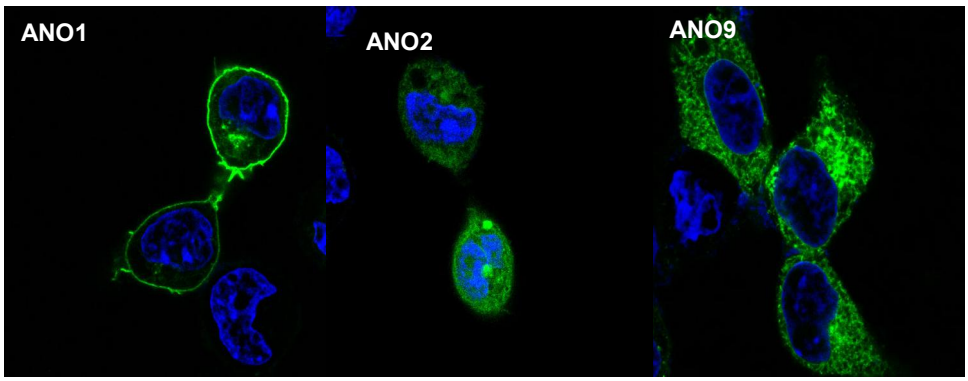

Figure 7. ANO1, ANO2 and ANO9 expression and subcellular localization

Immunofluorescence detection of HEK293T cell line transiently over expressing DAPI nuclear stained (blue) and GFP-tagged ANO1/ANO2/ANO9 (green) overlay.

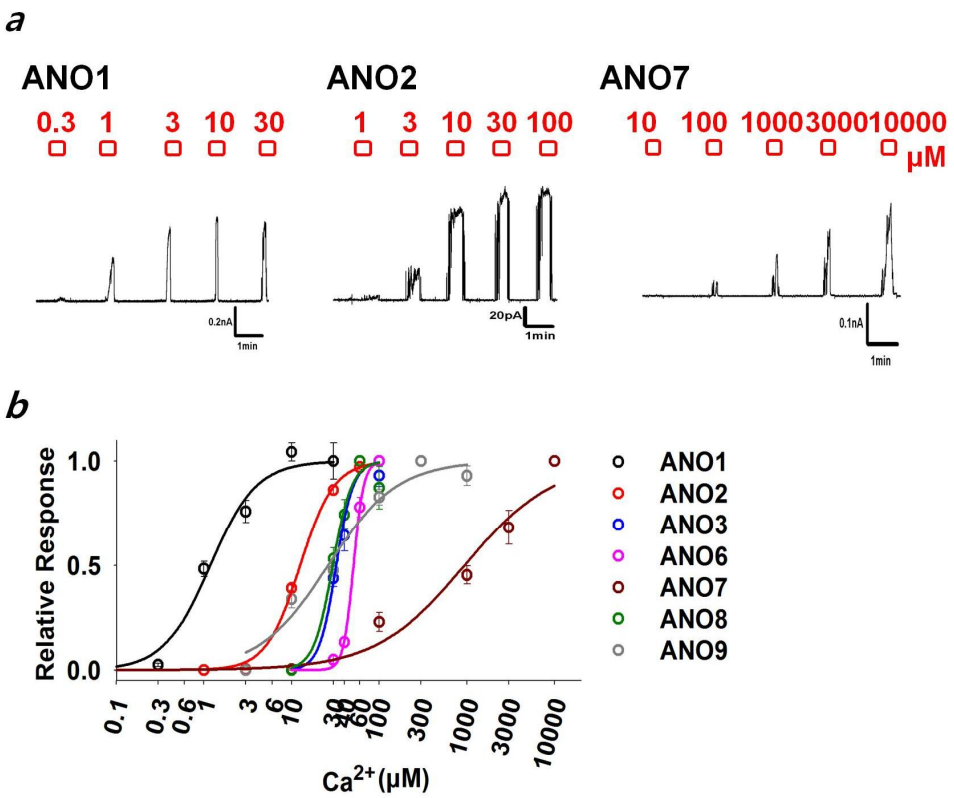

Figure 8. Ca^{2+} sensitivity at +80mV of the ANO1-3 and ANO6-9

(a) Example traces of channel currents of inside-out patches isolated from HEK293Tcells transfected with ANO1, ANO2 and ANO7. Holding potential (E_h)=+80mV. (b) Concentration-response relationships of channel currents of ANO1-3 and ANO6-9 activated by various concentrations of Ca^{2+}. Each current is normalized to the maximal response. Lines are fitted to the Hill equation, $I/I_{max}=1/(1+[Ca^{2+}]/EC_{50})^n$. EC_{50}s (in μM) for ANO1 (black circle), ANO2 (red circle), ANO3 (blue circle), ANO6 (pink circle), ANO7 (brown circle), ANO8 (green circle) and ANO9 (gray circle) were 0.7 (n=11), 9.8 (n=6), 32.2 (n=8), 50.7 (n=7), 935 (n=7), 29 (n=7), 25 (n=12), respectively.

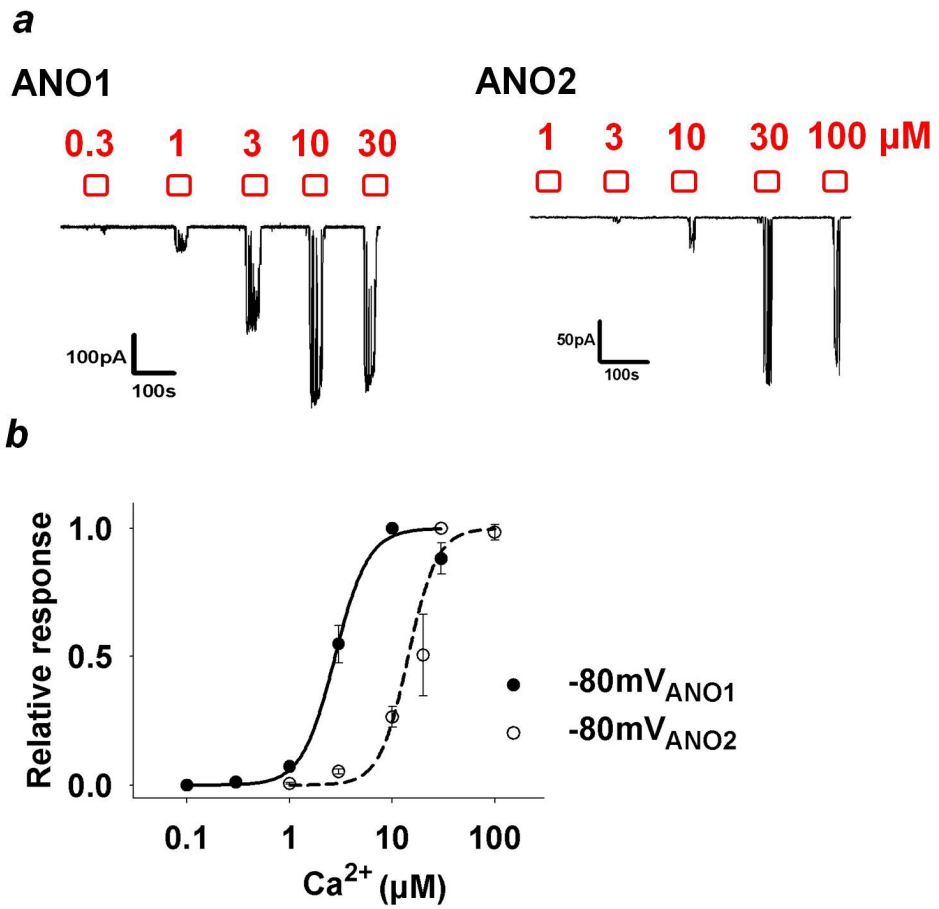

Figure 9. Ca^{2+} sensitivity at -80mV of the ANO1 and ANO2

(a) Example traces of channel currents of inside-out patches isolated from HEK293T cells transfected with ANO1 and ANO2. Holding potential (E_h)=-80mV. (b) Concentration-response relationships of channel currents of ANO1 and ANO2 activated by various concentrations of Ca^{2+}. Each current is normalized to the maximal response. Lines are fitted to the Hill equation, $I/I_{max}=1/(1+[Ca^{2+}]/EC_{50})^n$. EC_{50}s (in μM) for ANO1 (black circle), ANO2 (dashed circle) were 2.77 (n=5), 14.33 (n=8), respectively.

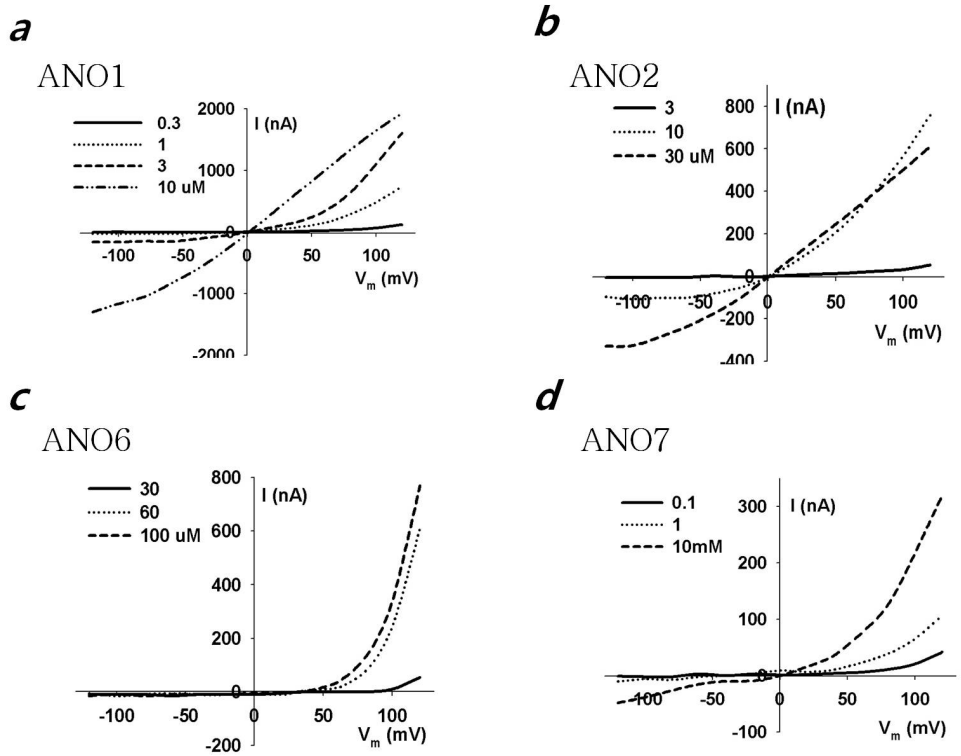

Figure 10. The I/V curves of ANO1, 2, 6 and 7 at various concentration of Ca^{2+}

(a) Current-voltage relationships of ANO1, (b) ANO2, (c) ANO6 and (d) ANO7 at various concentration of Ca^{2+}.

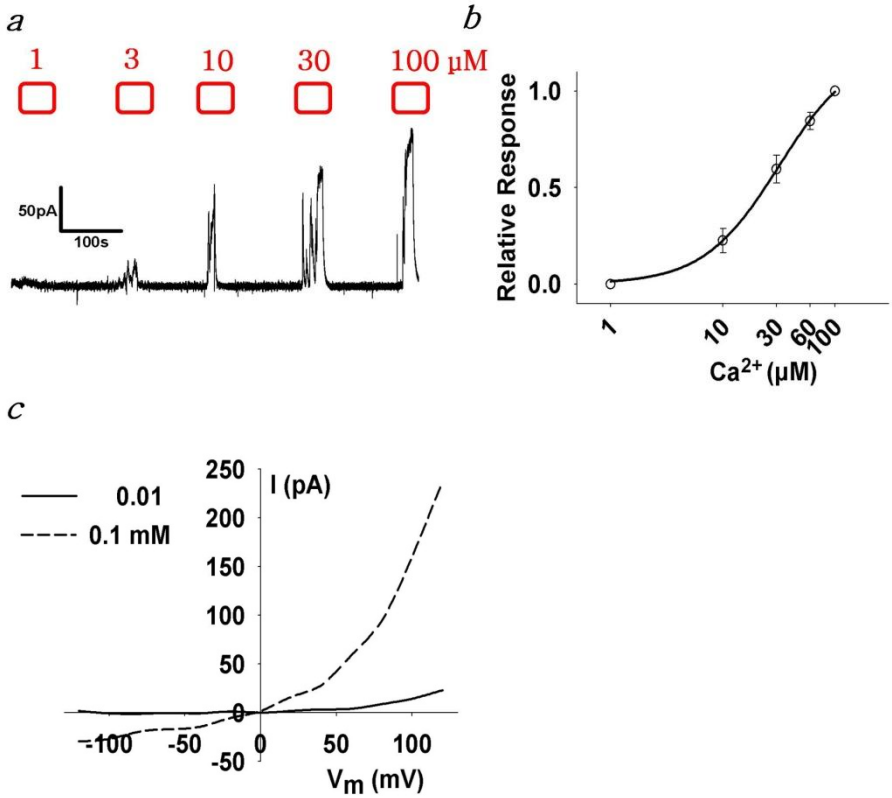

Figure 11. Ca^{2+} sensitivity at +80mV of the Subduced

(a) Example traces of channel currents of inside-out patches isolated from HEK293Tcells transfected with the Subduced. Holding potential (E_h)=+80mV. (b) Concentration-response relationships of channel currents of Subduced activated by various concentrations of Ca^{2+}. Each current is normalized to the maximal response. Lines are fitted to the Hill equation, $I/I_{max}=1/(1+[Ca^{2+}]/EC_{50})^n$. EC_{50} (in μM) for Subduced was 31.5 (n=6). (c) current-voltage relationship of Subduced at various concentration of Ca^{2+}.

1.2. Screen for putative common Ca^{2+}-binding regions in ANO1 and ANO2

Because of the absence of any Ca^{2+} binding motifs such as EF-hand, IQ-motif from ANO1 primary sequence, we chose some intracellular sites where there are rich negative charged amino acids or they resemble the E/F hand motif to find the potential intracellular Ca^{2+}-binding sites in the ANO1 sequence (Figure 12 and 13). The first site is the Glu- and Asp-rich (E/D rich) region spanning aa121~147 in the N-terminus. A deletion mutant (aa121~148) in E/D rich region was not expressed in the membrane and no currents were observed. However, mutants having nine Asp or Glu residues replaced with Asn or Gln in the E/D rich region (ED9) elicited currents with EC_{50} values comparable to that of wild-type (Figure 13a, b). The second site (285-**D**G**D**Y**E**GDNV**E**FND-297) in the N-terminus shares high homology with the Ca^{2+}-binding signature sequence of the EF-hand (-**D**x**D**x**D**Gxxxxx**E**-) of calmodulin (Xiong LW et al., 2010, Gifford JL et al., 2007). Replacing all four Asp or Glu residues with Ala shifted the EC_{50} for Ca^{2+} to 0.77 μM (Figure 13b). The third potential Ca^{2+} binding site is located in the first intracellular loop (ICL1) between TM2 and TM3. This site has five consecutive Glu residues (444-**EEEEE**AVK**D**HPRA**E**-457), which are loosely aligned with the Ca^{2+}-bowl region of large conductance Ca^{2+}-activated K^+ channel (Bian S et al., 2001, Yuan P et al., 2010). A

deletion mutant (444-EEEEE-448) in this region had an EC_{50} of 1.41 μM (Figure13a, b) likewise previous report (Xiao Q et al., 2011). Recently, a revised topology of ANO1 has been proposed in an intracellular loop which was previously thought to be extracellular. Moreover, $_{702}$EYMEM$_{706}$ in this 3rd intracellular loop (ICL3) contributes to Ca^{2+} gating with being conserved among all members of Anoctamin (Yu K et al., 2012). The dose-response curve of ICL3 deletion mutant was shifted dramatically to the right (EC50=308 μM, n=11) and currents rarely showed a saturation up to 10mM Ca^{2+} (Figure 13a, b). These results suggest that Ca^{2+} binds the ICL3 region of ANO1.

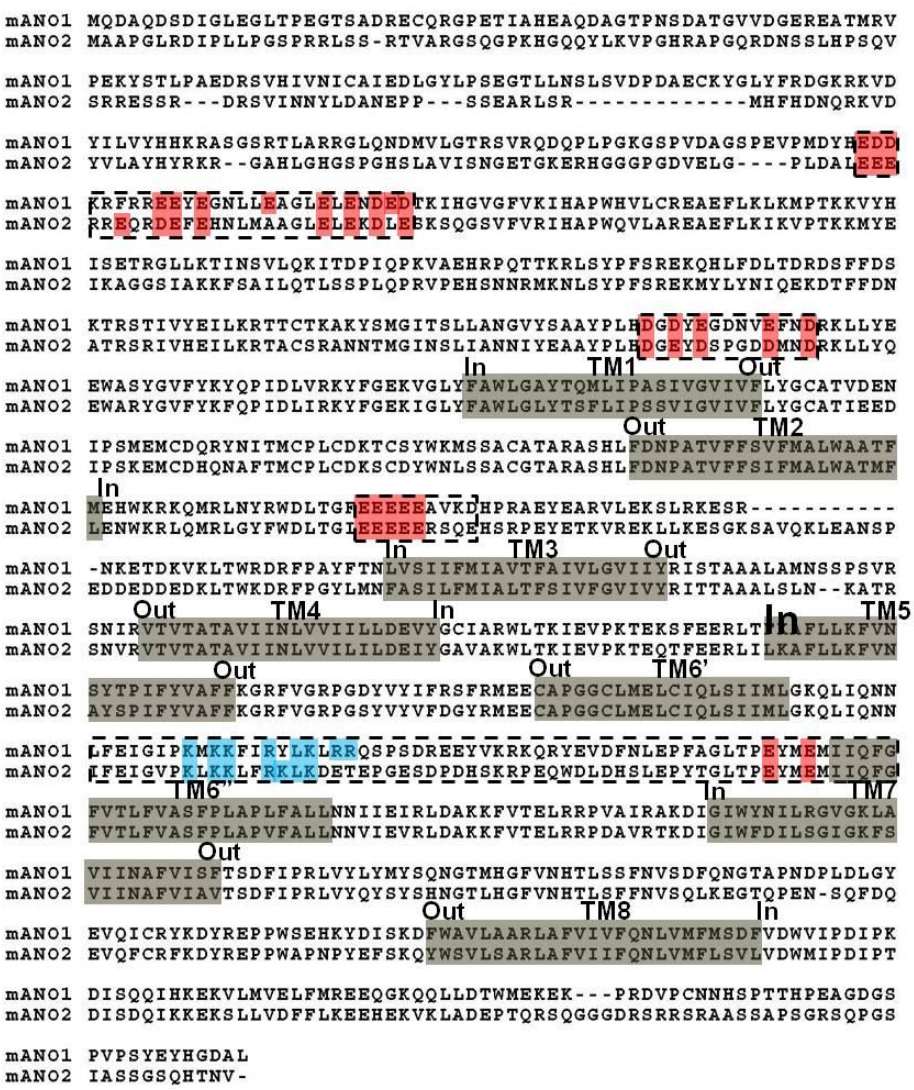

Figure 12. Sequence alignment between ANO1 and ANO2.

Highly conserved acidic residues that are likely to be bound with the intracellular Ca^{2+} are highlighted in red. Highly conserved basic residues are also highlighted in blue. In addition, putative transmembrane (TM) segments are highlighted in cyan.

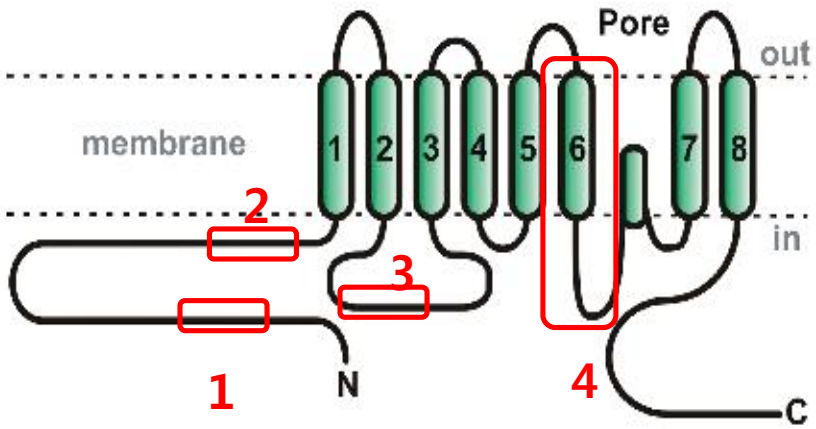

1. ED rich

2. EF-hand like region

3. Calcium bowl-like region

4. 3rd intracelluar loop (ICL3)

Figure 13. Potential common calcium-binding residues of ANO1 and ANO2

Topology of ANO1. ED rich region indicates Glu, and Asp rich region in the N-terminus; EF-hand like region indicates high homology region with the Ca^{2+}-binding signature sequence of the EF-hand (DxDxDGxxxxxE) of calmodulin in the N-terminus; Calcium ball-like region indicates five consecutive Glu residues in the first intracellular loop (ICL1); 3rd intracellular loop (ICL3) indicate the third loop that is thought to be intracellular.

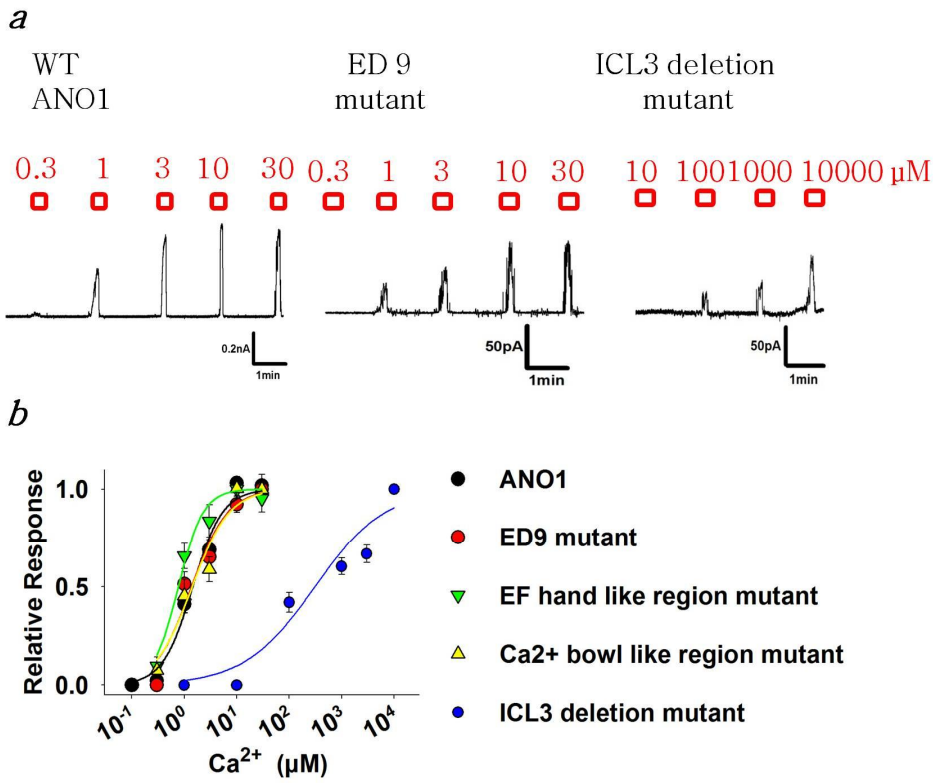

Figure 14. Screen for common calcium-binding residues of ANO1 and ANO2

(a) Example traces of channel currents of inside-out patches isolated from ANO1 and a ANO1 deletion mutant-transfected HEK293T cells. ED9 mutant of 120-H**QNN**KRFRR**QQ**YQGNLLEAGL**Q**L**Q**ND**Q**DT-148, ICL3 deletion mutant of the third intracellular loop region. Holding potential (E_h)=+80mV. (b) Concentration-response relationships of channel currents of ANO1, and ANO1 mutants activated by various concentrations of Ca^{2+}. Each current is normalized to the maximal response. Lines are fitted to the Hill equation, $I/Imax=1/(1+[Ca^{2+}]/EC_{50})^n$. EC_{50}s (in μM) for ANO1 (black circle) and ANO1 mutants were 0.7 (n=11), ED9 mutant (red circle), 1.37 (n=9), 285-**A**GA**A**YA**A**GA-291 ((EF hand-like region mutant (green reverse

triangle), 0.77 (n=8)), Δ5E ((Ca^{2+}-bowl like region mutant (yellow triangle), 1.41 (n=9)), ΔICL3 (ICL3 deletion mutant (blue circle), 308 (n=10)), respectively.

2. Structural prediction of the ICL3 region of ANO1/2

2.1. Homologous models of ANO1/2

In an attempt to gain insight into the structure of this region, we also researched for crystal structures homologous to the ICL3 segment from the protein MODWEB server, an automated homology-modeling program (http://salilab.org/modweb). This search revealed that a partial segment (residues 606~663) of the ICL3 of ANO2 is homologous to a part of crystal structure (PDB ID: 3QBU) of a peptidoglycan deacetylase of *Helicobacter pylori,* with a 46% sequence identity (not including gaps) (Figure 15a). The model was considered reliable because the model satisfied GA341 (0.78, the score based on statistical potentials higher than the pre-specified cutoff; 0.7) and z-DOPE (-0.6, an atomic distance-dependent statistical potential from a sample of native structures, reliable if z-DOPE < 0). Structure homology modeling (PyMOL) of the ICL3 segment of ANO2 showed two parallel-helices in close proximity, one of which is the Lys- and Arg-rich helix. Interestingly, the other helix contains the two Glu residues which had been suggested to be important for Ca^{2+} sensitivity in ANO1 (Yu K et al., 2012)

(Figure 15b). Because these two Glu residues appear critical for Ca^{2+}-induced activation (below), we called this helix the 'Ca^{2+} sensor helix'. For the counterpart helix that appears important for interacting with the Ca^{2+}-sensor helix, we called the 'reference helix'. The two helices were linked by ~25 amino acids (Figure15c). Because ICL3 region of ANO1 and ANO2 has a high sequence similarity of 51.7% (Figure15c), we also modeled an ANO1 structure (amino acids 653-711) using the backbone of the ANO2 ICL3 region as template. Overall, the resulting structure of ANO1 resembled that of ANO2 (Fiugre 15d).

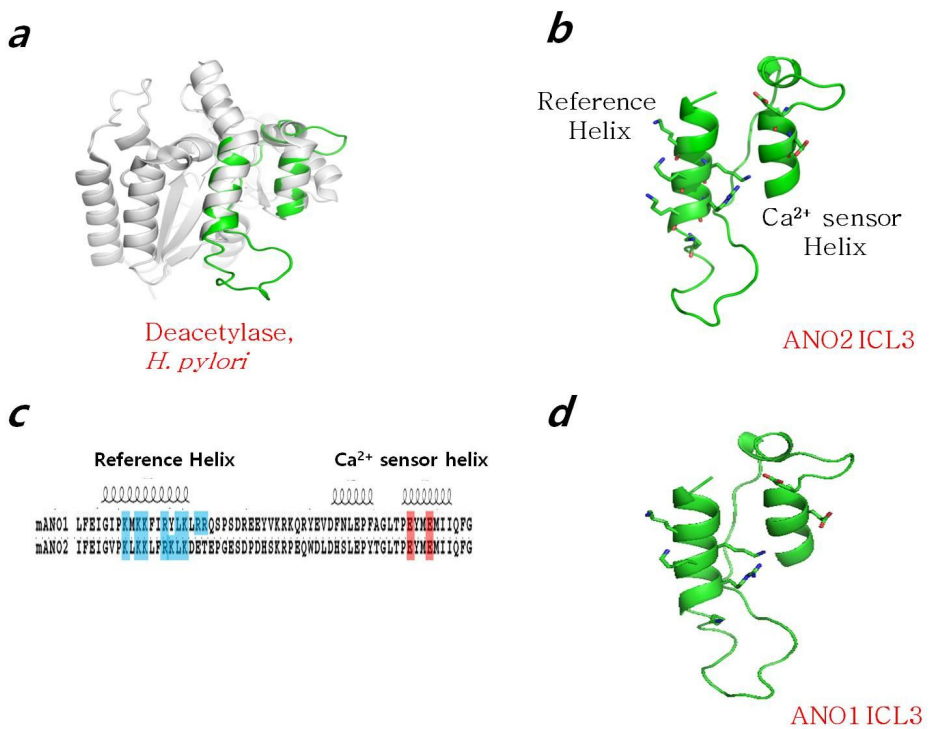

Figure 15. Homology models of the ICL3 regions of ANO1 and ANO2

(**a**) A crystal structure of a part of a peptidoglycan deacetylase of *Helicobacter pylori* that shares structural homology with the ICL3 region of ANO2

(**b**) A homology model of the ICL3 of ANO2. Structure of the ICL3 region of ANO2 was modeled using the backbone coordinates of the deacetylase of *Helicobacter pylori* as a template. Side-chains of Arg and Lys are shown in stick. Blue and red atoms in the side chains represent nitrogen and oxygen atoms, respectively.

(**c**) Alignment of ICL3 amino acid sequence in ANO1 and ANO2 indicates sequence identity for ANO1/ANO2 of 51.7%

(**d**) A homology model of the ICL3 of ANO1. Structure of the ICL3 region of ANO1 was modeled using the backbone coordinates of the ICL3 region of ANO2 as a template.

2.2. Secondary structure prediction of ANO1

To investigate the molecular basis of Ca^{2+}-induced activation by this region in detail, we examined the secondary structure and topology of ANO1. We utilized 12 different transmembrane (TM) prediction programs (Yu K et al., 2012) as well as nine different algorithms of secondary structure prediction (XtalPred and Biology Workbench, PELE). According to these programs, there was a consensus among structural predictions. Overall, the predicted ANO1 secondary structures, up to the C-terminus of TM5 (residues 1~604), were similar across the programs. From the end of TM5 towards the C-terminus, the secondary structure predictions were different among programs. However, a number of these algorithms

predicted that TM5 is followed by two helices with a short break (residues 634-671). The upper helix (residues 634~654) is predicted by some programs as a TM segment because it has 12 hydrophobic amino acids (Figure 16). Interestingly, the lower helix (residues 656~671) contains multiple positively charged Lys or Arg residues. This is followed by two shorter helices, residues 680-690 and 700-710 before TM6. (Figure 16)

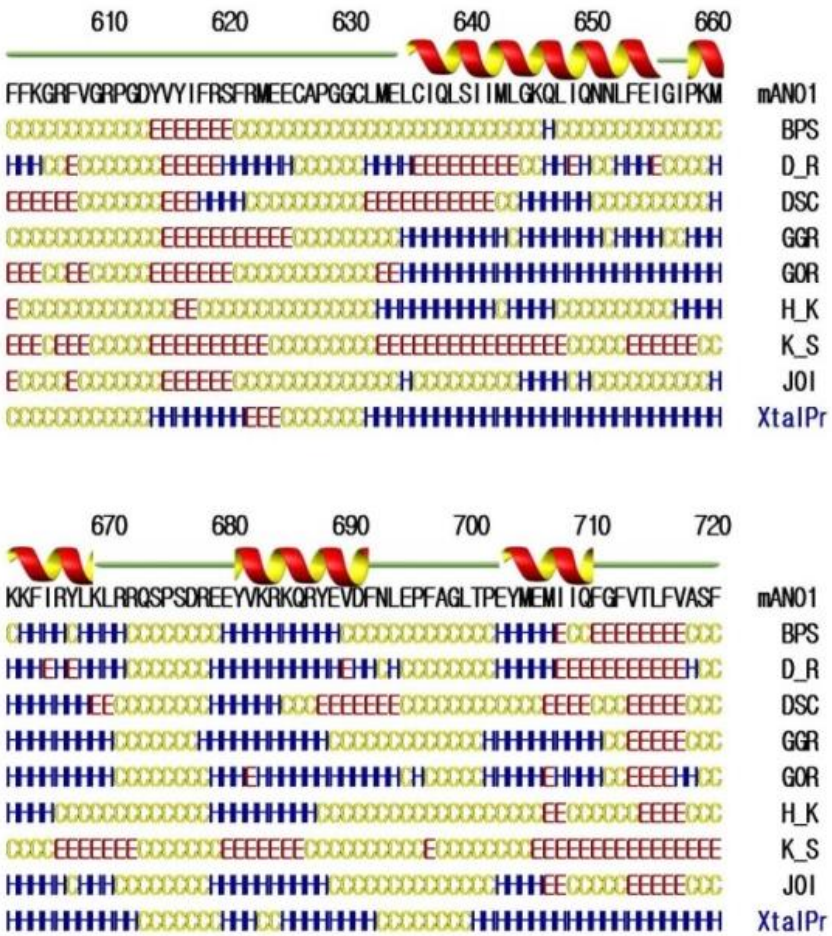

Figure 16. Secondary structure prediction of ANO1 by eight algorithms in *PELE* and *XtalPred* program

Legends of *XtalPred* program are depicted as shown in *PELE*. H – alpha helices, E – beta strands, C – coil,

2.3. Homologous models of other ANO channels

When the reference helix regions were aligned, ANO1 and ANO2 isoforms had four and five basic residues, respectively. All other ANO isoforms had 1~3 Arg or Lys residues in this region. The two Glu residues in the Ca^{2+}-sensor helix were well conserved throughout the ANO isoforms. The reference helix and linker region between the two helices were variable across ANO family members (Figure 17).

We then attempted to extract the structures of ICL3 regions of other ANO channels from the ANO2 backbone. However, attempts to model these structures were not successful, primarily because amino acid sequences in this region of other ANO family members were not predicted to form a helix. Thus, structures of other ANO channels were considered to be grossly different from those of ANO1 and 2 as well as the Ca^{2+} sensitivity and voltage dependency of ANO1 and 2. Indeed, structure homology search also led to the finding that the structure of the ICL3 region of ANO6 was similar to that of a hypothetical protein PH1257 from *Pyrococcus horikoshii* OT3 (PDB ID: 2D13) with a 50% sequence identity. This partial structure of ANO6 is grossly different from those of ANO1 and ANO2 in that the reference helix is absent (Figure 18). Likewise, the

structure of the ICL3 region of ANO7 resembles that of human chromodomain Y-like protein 2 (PDB ID: 4HAE), with a 39% sequence identity (Figure 18). This structural model of ANO7 does not resemble those of ANO1 and 2 because the two parallel helices in the ICL3 region are also absent although ANO7 is activated by high Ca^{2+} concentration in cytosol. These results suggest that the helix-loop-helix structure of the ICL3 regions appears specific only to ANO1 and 2, and may not be applicable to other ANO channels.

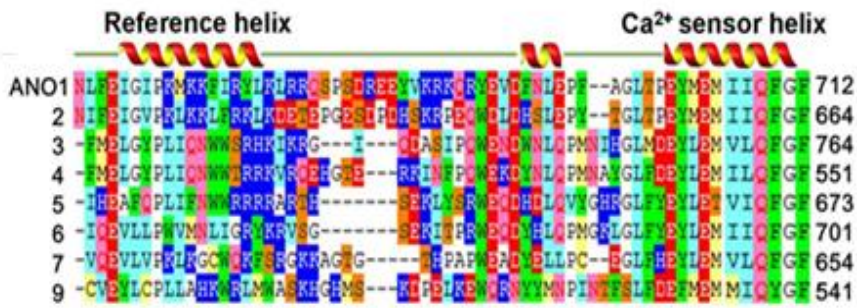

Figure 17. Sequence alignment of the ICL3 regions from ANO1 and its paralogs

Helices are shown only for ANO1 and ANO2.

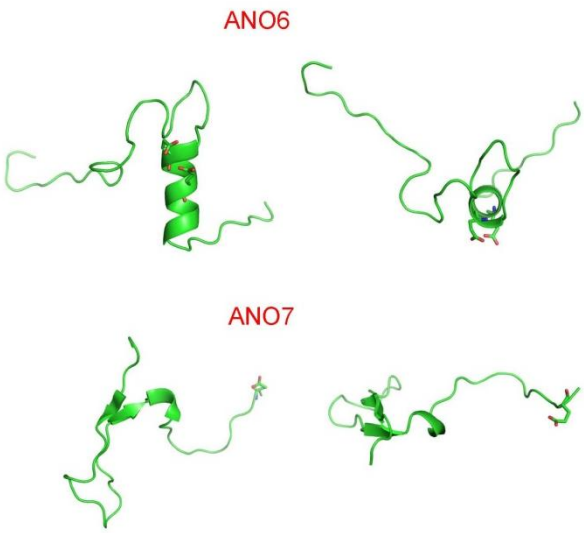

Figure 18. Homology models of the ICL3 regions of ANO6 and ANO7
The structures of ICL3 regions of ANO6 and ANO7 are modeled using the backbone coordinates of PH1257 from *Pyrococcus horikoshii* OT3 and human chromodomain Y-like protein 2, respectively, as templates.

3. Gating mechanism by Ca^{2+} in two helices of ICL3 region

3.1. Binding of the two helices in Ca^{2+} dependent manner

Because the two parallel helices in the ICL3 region of ANO1 have amino acids with opposite charges, these opposing charges may engage in the activation of ANO1 by Ca^{2+} (Fig. 19). At first we performed circular dichroism spectroscopy with synthetic peptides spanning the reference helix regions of ANO1 (651-NLFEIGIP**K**M**KK**FI**R**YL**K**L**RR**-671) and ANO2 (604-IFEIGVP**K**L**KK**LF**RK**L**K**D-621) to confirm whether the reference helix of ANO1 and ANO2 forms an α-helix. The two peptides of ANO1 and ANO2 had a typical circular dichroism spectrum of an α-helix with a positive band around 192 nm and negative bands around 208 and 222 nm (Fig. 20).

Also, in order to investigate a Ca^{2+}-dependent physical interaction between the two helices, we performed surface plasmon resonance (SPR). A peptide segment (692-NLEPFAGLTPEYMEM-706) spanning the Ca^{2+} sensor helix of ANO1 was synthesized, biotinylated at the N-terminus, and immobilized on a Streptavidin-coated gold sensor chip. Subsequently, a synthetic peptide spanning the reference helix of ANO1 (651-NLFEIGIP**K**M**KK**FI**R**YL**K**L**RR**-671) was passed over the immobilized Ca^{2+} sensor helix. In the absence of Ca^{2+}, the reference-helix peptide interacted strongly with the Ca^{2+} sensor helix (Fig. 21a). Ca^{2+} (0.4 – 2 mM)

produced a dose-dependent reduction in the interaction between the two synthetic helix peptides. A mutant of the reference helix peptide in which all Lys and Arg residues were replaced with Gly (651-NLFEIGIP**G**M**GG**FI**G**YL**G**L**GG**-671) failed to show any interaction with the Ca^{2+} sensor helix peptide regardless of Ca^{2+} concentration (Fig. 21b). In previous electrophysiological studies, the synthetic peptides were also used to confirm that they are interacted with a specific site in channel protein (Ferrer-Montiel et al., 1998; Planells-Cases et al., 2000) So, we applied the reference-helix and Ca^{2+} sensor-helix peptides to isolated inside-out patches of HEK 293T cells transfected with ANO1, to see if the peptides antagonized Ca^{2+} in activating ANO1. Indeed, application of 4 μM reference helix-peptide or 10 μM Ca^{2+} sensor helix peptide markedly blocked Ca^{2+}-induced ANO1 currents. In contrast, the Gly-mutant reference-helix peptide failed to block the Ca^{2+}-induced ANO1 currents (Fig. 22a, b). Overall, these results clearly indicate that the two helices interact directly with each other in a Ca^{2+} dependent manner.

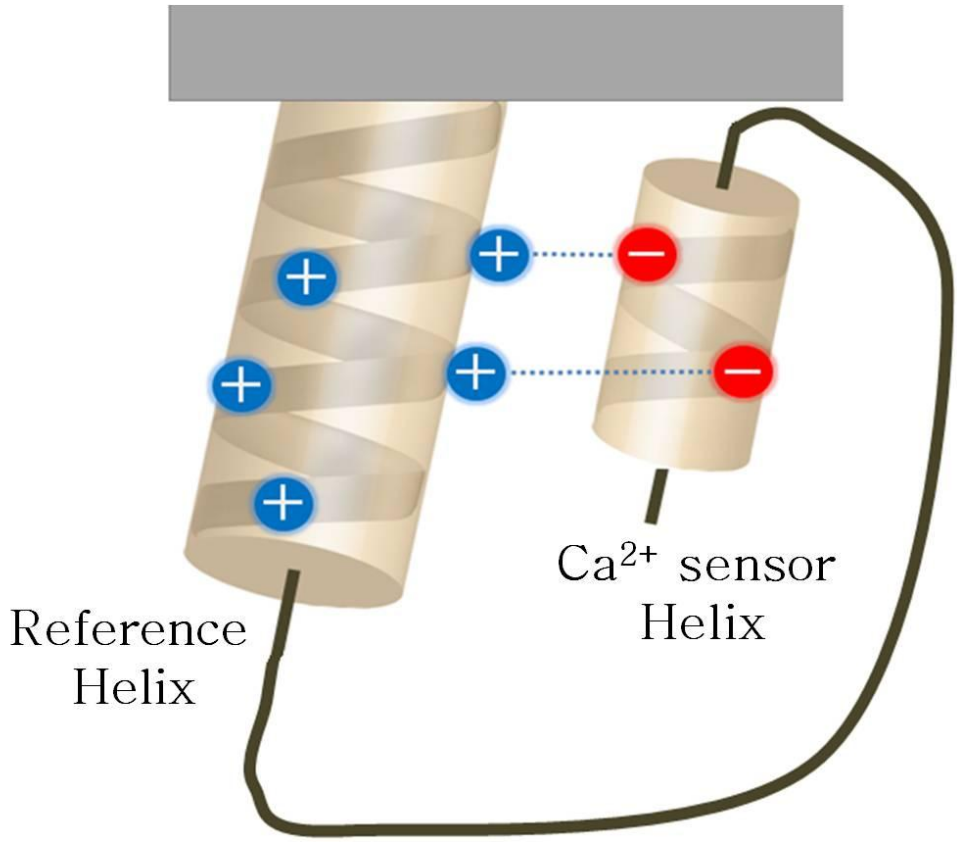

Figure 19. Schematic illustrating the putative structure of the two helices in ICL3 of ANO1

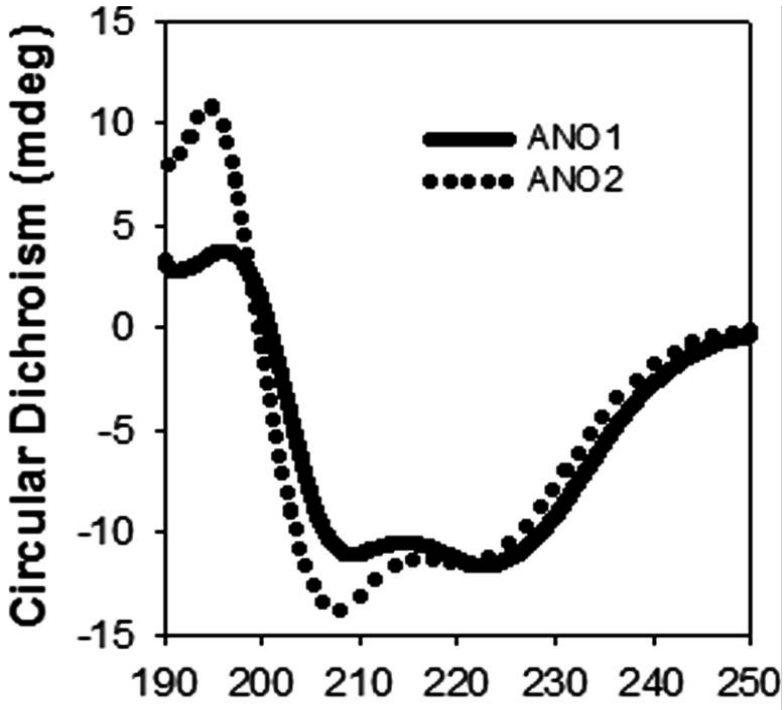

Figure 20. Circular dichroism spectra of two reference helix peptides of ANO1 and ANO2

The two peptides that span the reference helices in the ICL3 regions of ANO1 and ANO2 were 651-NLFEIGIP**K**M**KK**FI**R**YL**K**L**RR**-671 and 604-IFEIGVP**K**L**KK**LF**RK**L**K**D-621, respectively. Note a typical α-helical character with a positive band around 192 nm and negative bands around 208 and 222 nm.

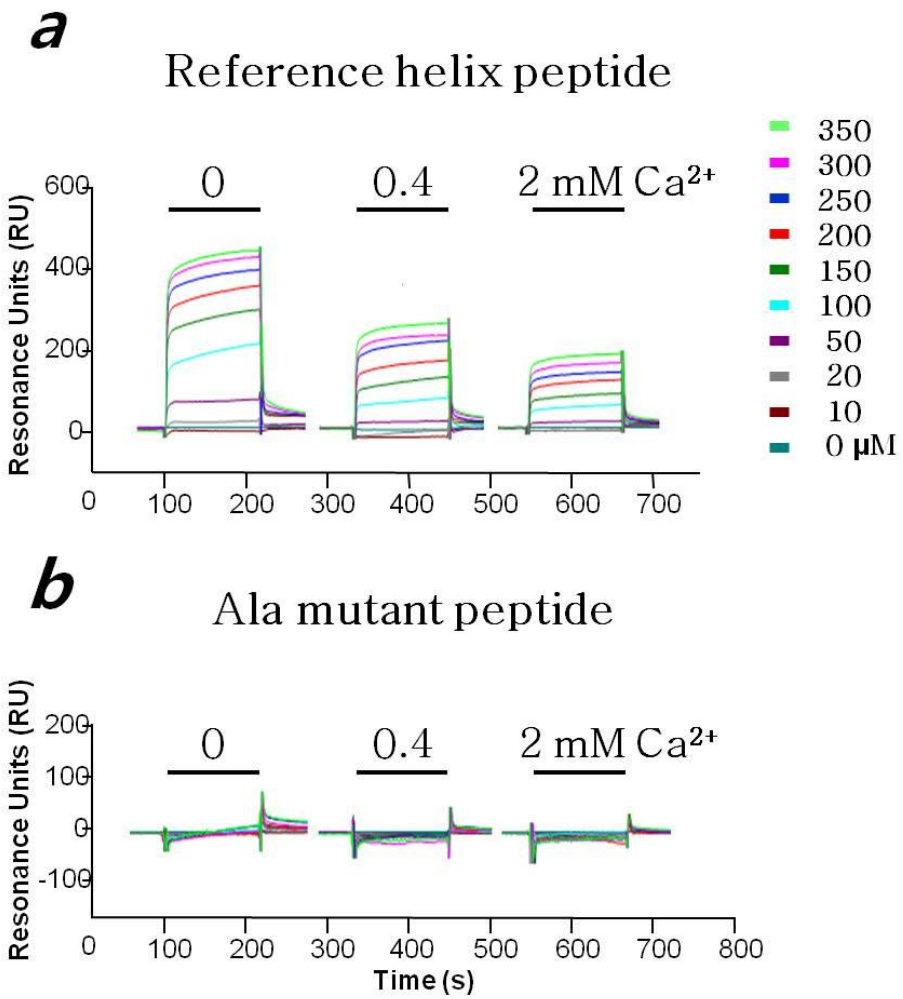

Figure 21. The reference helix of the ICL3 region interacts with the Ca^{2+} sensor helix in a Ca^{2+} -dependent way

Physical interaction between the reference helix and a Ca^{2+} sensor helix was assessed with a surface plasmon resonance assay. Biotinylated Ca^{2+} sensor helix peptide (692-NLEPFAGLTPEYMEM-706) was immobilized on a streptavidin-coated gold sensor chip. Resonance intensities were measured after solutions containing 0, 0.4, and 2.0 mM Ca^{2+} and various concentrations of reference helix peptide (651-NLFEIGIP**K**M**KK**FI**R**YL**K**L**RR**-671) **(a)** or its Ala-substituted mutants

(651-NLFEIGIP**A**M**AA**FI**A**YL**A**L**AA**-671) **(b)** were flowed through the gold chip. Note that the wild-type reference helix peptide shows a binding with the Ca^{2+} sensor helix in a Ca^{2+} -dependent manner **(a)**, which is not observed for the Ala-substituted mutant peptide **(b)**.

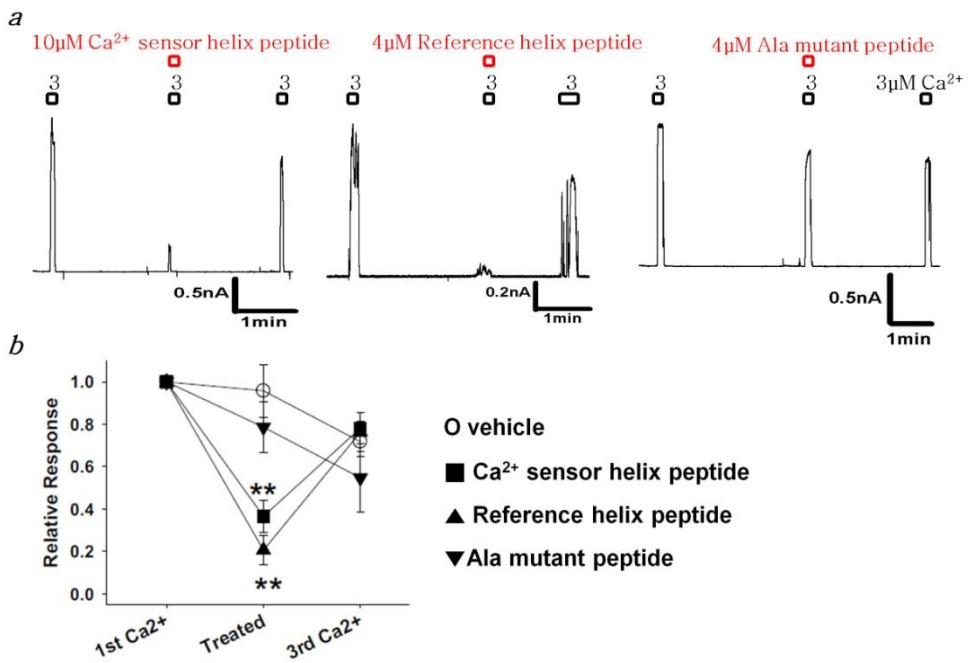

Figure 22. The reference helix of the ICL3 region interacts with the Ca^{2+} sensor helix in a Ca^{2+} -dependent way

(a) Example traces of channel currents of inside-out patches isolated from HEK293T cells transfected with ANO1. Ca^{2+}-induced ANO1 currents were blocked by bath application of both Ca^{2+} sensor helix peptide (692-NLEPFAGLTPEYMEM-706) and the reference helix peptide (651-NLFEIGIP**K**M**KK**FI**R**YL**K**L**RR**-671) to inside-out patches (*upper left and middle panel*) but not by the Ala-mutant peptide (651-NLFEIGIP**A**M**AA**FI**A**YL**A**L**AA**-671) (*upper right panel*). Ca^{2+} (3 μ M) was applied three times to inside-out patches of ANO1-transfected HEK 293T cells. At the second Ca^{2+} challenge, the peptides were also given.

E_h=+80 mV. (b) A summary plot of the effects of applications of reference helix and Ca^{2+} sensor helix peptide on Ca^{2+}-activated ANO1 currents. Currents amplitudes were normalized to the current amplitude obtained after of the first Ca^{2+} challenge. At the second Ca^{2+} challenge, reference helix peptide (*black circle*, **p<0.01 compared to the relative response of vehicle application, one-way ANOVA, Newman-Keuls post hoc test, n=13), Ala-replaced reference helix peptide (*black inverted triangle*, n=8), the Ca^{2+} sensor helix peptide (700-TPEYMEMIIQFGF-712) (*black square*, **p<0.01 compared to the relative response of vehicle application , one way ANOVA, Newman-Keuls post hoc test, n=7), and vehicle (white circle, n=8) were also applied.

3.2. Alteration of Ca^{2+} sensitivity by mutations in the two helices of ICL3

To determine whether charged residues in the two helices are essential for the ANO1 activation by Ca^{2+}, we constructed ANO1 and ANO2 mutants whose Arg or Lys residues in the reference helix were replaced with non-charged residues (Ala, Gln, or Gly) and ICL3 region were deleted (Fig. 23a, b). Replacement of single Lys residues to Gln in the upper part of the reference helix such as 659-KMKK-662 mutant caused a rightward shift of EC_{50} values, ranging from 3.6 to 6.1 μM (Fig. 23a). When all three Lys residues in the region were replaced with Gly (659-GMGG-662), the EC_{50} increased to 22.8 μM (Fig. 23a). Replacement of Arg or Lys residues with Gly in the lower part of the reference helix such as 665-GYLG-668 mutant shifted the EC_{50} value to 6.2 μM (Fig. 23a). Furthermore, deletion (ΔKMKKFIRYLK) of the reference helix changed the EC_{50} values to 51.0 μM (Fig. 23a). A mutation of the two Glu residues in the Ca^{2+} sensor helix (702-EYME/QYMQ-705) elicited a four-order magnitude of rightward shift in 11.3 mM of EC_{50} (Fig. 23a). Likewise, mutations in the reference helix of ANO2 also reduced the potency of Ca^{2+} in opening ANO2. Replacing all three Lys residues to Gln in the upper part of the reference helix increased the EC_{50} from 9.8 to 50.2 μM (Fig. 23b). In addition, replacement to Gly of all charged residues in the reference helix (611-GLGGLFGGLG-620)

caused a dramatic rightward shift of 349 μM of EC_{50} (Fig. 23b). Mutation of the two Glu residues in the Ca^{2+} sensor helix (654-EYME/AYMA-657) elicited a three-order magnitude of rightward shift in 3.3 mM of EC_{50} (Fig. 23b). These results indicate that charged residues in the two helices both of ANO1 and ANO2 were significantly implicated in Ca^{2+}-dependent activation.

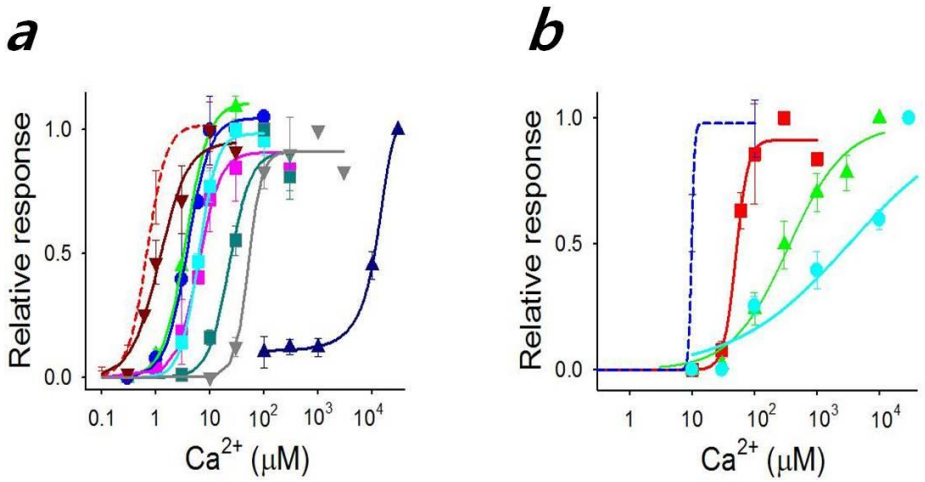

Figure 23. Mutations in the ICL3 regions of ANO1 and ANO2 shift the sensitivity of Ca^{2+}-dependent activation

(a) Replacement of Arg, Lys, or Glu residue with Ala, Gly, or Gln residue in the reference and Ca^{2+} sensor helices caused rightward shifts in the dose-response relationship curve of ANO1. EC_{50}s (in μM) for ANO1 mutants were 659-QMKK-662 (pink square, 6.1, n=4), KMQK (blue circle, 4.7, n=5), KMKQ (green triangle, 3.6, n=6), GMGG (dark green square, 22.8, n=6), 665-GYLG-668 (light blue square, 6.2, n=6), deletion of 659 KMKKFIRYLK-668 (gray inverted triangle, 51.0, n=9), 670-GGQ-672 (brown inverted triangle, 1.2, n=7), and 702-QYMQ-705 (blue square 11260,

n=7). The dose-response curve of wild-type (WT) ANO1 is the same as shown in Fig. (red line).

(b) Mutations in the ICL3 region of ANO2 also shifted dose-response curves rightward. EC_{50}s were 611-QLQQ-614 (red square, 50.2 μM, n=7), 611-GLGGLFGGLG-620 (green triangle, 348.9 μM, n=8), and 654-AYMA-657 (light blue circle, 3.3 mM, n=6). The dose response curve of WT ANO2 (blue line) is same as shown in Fig.

3.3 Action of E_{act} on the reference helix peptide

E_{act}, a synthetic agonist of ANO1, was synthesized for the purpose of treating cystic fibrosis in an attempt to bypass dysfunctioning CFTR channel (Namkung W et al. 2011). Even though E_{act} was known to activate ANO1, the activation mechanism is not known. We therefore hypothesized that E_{act} also acts on the ICL3 region. Application of 1 μM E_{act} to the bath of inside-out patch activated ANO1, just like Ca^{2+} (Fig. 24). In addition, maximal Eact (10 μM) activated the Δ5E ANO1 mutant that deleted the Ca^{2+} bowl-like region in ICL1 (Fig. 24). E_{act} also activated 285-AGAYAGA-291 mutant that replaced acidic amino acids in the EF-hand-like region in the N-terminus (data not shown). However, when applied to ΔICL3, the deletion mutant of ANO1 in the ICL3 region, E_{act} failed to activate, whereas 10 mM Ca^{2+} evoked a small current (Fig. 24). In addition, E_{act} failed to activate both the QYMQ (data not shown) and 659-QMQQFIAYLQ-668 mutants that neutralized charges in the Ca^{2+} sensor helix and reference helix, respectively (Fig. 24).

We then applied the two helix peptides to see if these peptides compete with Eact in activating ANO1. When 10 μM Ca^{2+}-sensor helix peptide was applied together with 1 μM E_{act} to inside-out patches from ANO1-transfected cells, the peptide failed to inhibit Eact-activated currents (Fig. 25a). In contrast, when 4 μM reference helix peptide was applied together

with E_{act}, the peptide significantly inhibited the Eact activated ANO1 currents (Fig. 25b) ($p<0.05$, one-way ANOVA, Newman-Keuls post hoc test, n=5~14). However, the Ala substituted reference helix peptide failed to inhibit the E_{act} activated ANO1 currents (Fig. 25a, b). These results clearly suggest that E_{act} acts on the reference helix in the ICL3 region as Ca^{2+}.

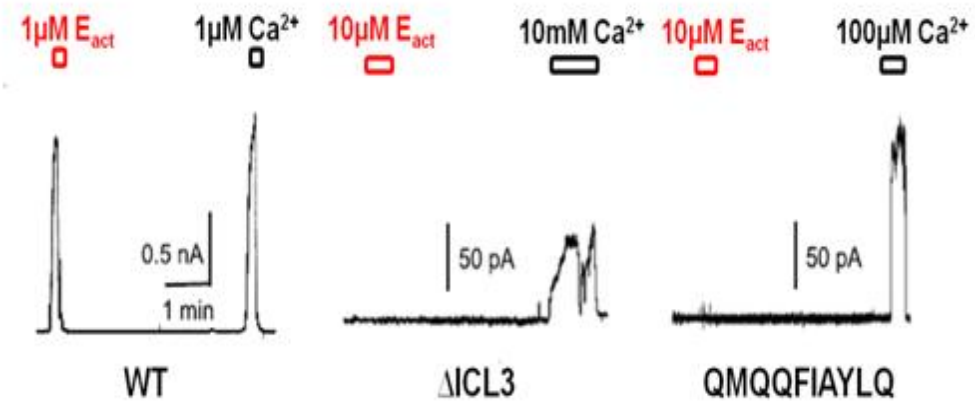

Figure 24. Action on the ICL3 region of E_{act}, a synthetic agonist of ANO1

Example traces depicting activation by E_{act} of WT ANO1 (left), ΔICL3 (middle), and 659- QMQQFIAYLQ-668 mutant(right).

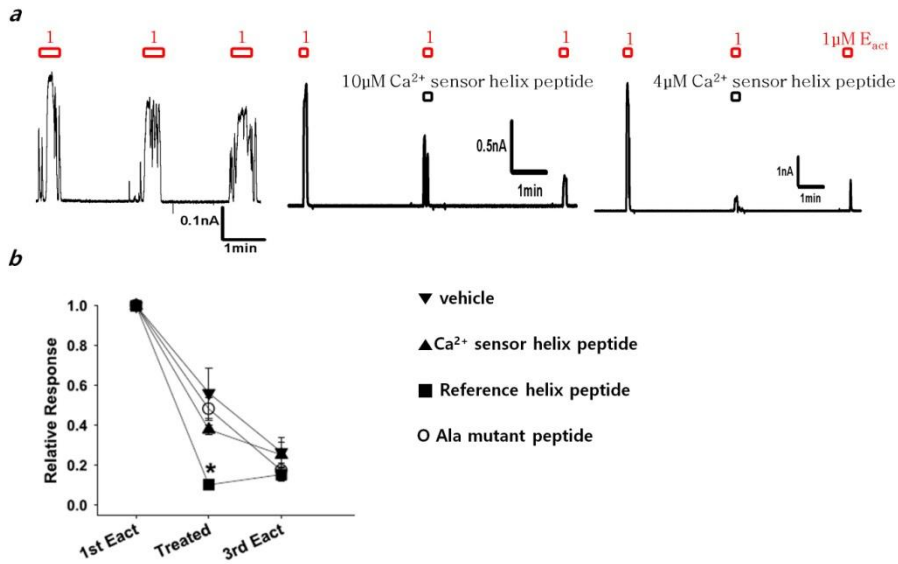

Figure 25. Action region of E_{act} on the reference helix in the ICL3

Example traces of Eact-induced ANO1 currents, which were blocked by bath application of the reference helix peptide (reference helix peptide, 651-NLFEIGIPKMKKFIRYLKLRR- 671, 4 μM, lower panel) but not by the Ca2+ sensor helix peptide (CSH peptide, 700- TPEYMEMIIQFGF-712, 10 μM, middle panel). To test the effects of peptide, 1 μM Eact was applied three times. At the second E_{act} challenge, each peptide was also applied. c A summary of the effects of applications of helix peptides on E_{act}-induced ANO1 currents. Current amplitudes were normalized to the current amplitude obtained after of the first E_{act} challenge. Reference helix peptide (black square, n=5), its Ala-mutant peptide (black inverted triangle, n=5), Ca^{2+} sensor helix peptide (black triangle, n=5), or vehicle (white circle, n=14) was applied at the second Eact challenge. *$p<0.05$ compared to the relative response of vehicle application, one-way ANOVA followed by Newman-Keuls post hoc test

3.4 Correlation between voltage and heat on ICL3 region

We reasoned that the positively charged residues in the reference helix may play a role in mediating voltage-dependent activation. Progressive replacement of Lys residues in the upper part of the reference helix shifted the half-maximal activation voltages ($V_{1/2}$) in G/V curves, an indication of voltage-independent activation, from −112 to +106 mV without changing the slopes (z=0.24~0.39) of the G–V curve (Fig. 26b). When the ICL3 region of ANO1 (residues 653~ 711) was deleted, the V1/2s of the G/V curves did not vary (+ 39.5~+77.3 mV) between 10 μM and 10 mM $[Ca^{2+}]_i$ (Fig. 26b), which contrasts to a 294-mV change in $V_{1/2}$ of the wild-type ANO1 (Fig. 26b). In addition, the slopes of G/V curves did not vary (z=0.32~0.46) upon deletion; the ICL3 region is not a site for voltage-induced activation.

Another activation stimulus for ANO1 is heat. Bath temperature greater than 44 °C is sufficient to open the ANO1 channel (Cho et al., 2012). Because the activation by Ca^{2+} and heat are synergistic, we tested whether the heat-induced ANO1 activation is also mediated by the ICL3 region. To eliminate activation by Ca^{2+}, we removed Ca^{2+} from the pipette solution (0 Ca^{2+} with 5 mM ethylene glycol tetraacetic acid (EGTA)) in a whole-cell recording (Fig 27a). Surprisingly, a mutant (ΔICL3) which hardly responded to sub-millimolar Ca^{2+} concentration elicited currents when the

temperature of bath solution was raised over 44 ℃ (Fig 27b). Thus, these results suggest that the activation mechanism of ANO1 by voltage and heat is different from that by Ca^{2+}.

Taken together, based on the above results, we predicted that, in the closed state, the two helices 'hold' together primarily due to the ionic interactions between positive and negative charges in the two helices (Fig. 28). However, as intracellular [Ca^{2+}] increases, Ca^{2+} binds and covers the Ca^{2+} sensor helix around the two Glu residues. These positive charges from the Ca^{2+} may break the ionic interaction between the two helices and repel the reference helix away from the Ca^{2+} sensor helix (Fig. 28). When the Ca^{2+} ions are removed, the Ca^{2+} sensor helix again moves closer to the reference helix (Fig. 28). This conformational change of the two helices would lead to a conformational change in the channel gate.

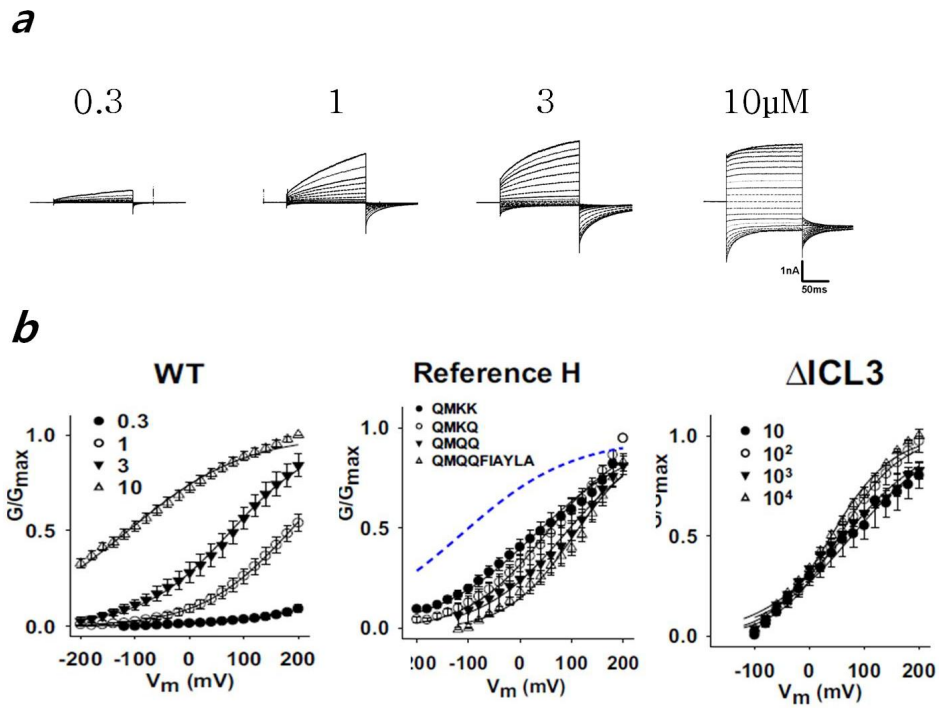

Figure 26. The two helices in the ICL3 region are dispensable for voltage-dependent ANO1 activation

(a) Current responses of WT ANO1 to voltage pulses (-200 to +200mV in 20mV increment) at 0.3, 1.0, 3.0, and 10 μM Ca^{2+} (upper). (b) G/Gmaxs at different $[Ca^{2+}]_i$ were plotted against membrane potential (Vm). G-V curves of various mutants in the reference helix at 10 μM $[Ca^{2+}]_i$ $[Ca2+]_i$ and an ICL3-deleted mutant (residues 653-711) of ANO1 at 10 μM ~10 mM $[Ca^{2+}]_i$. The G-V curve of WT ANO1 was the same as shown in Fig. a.

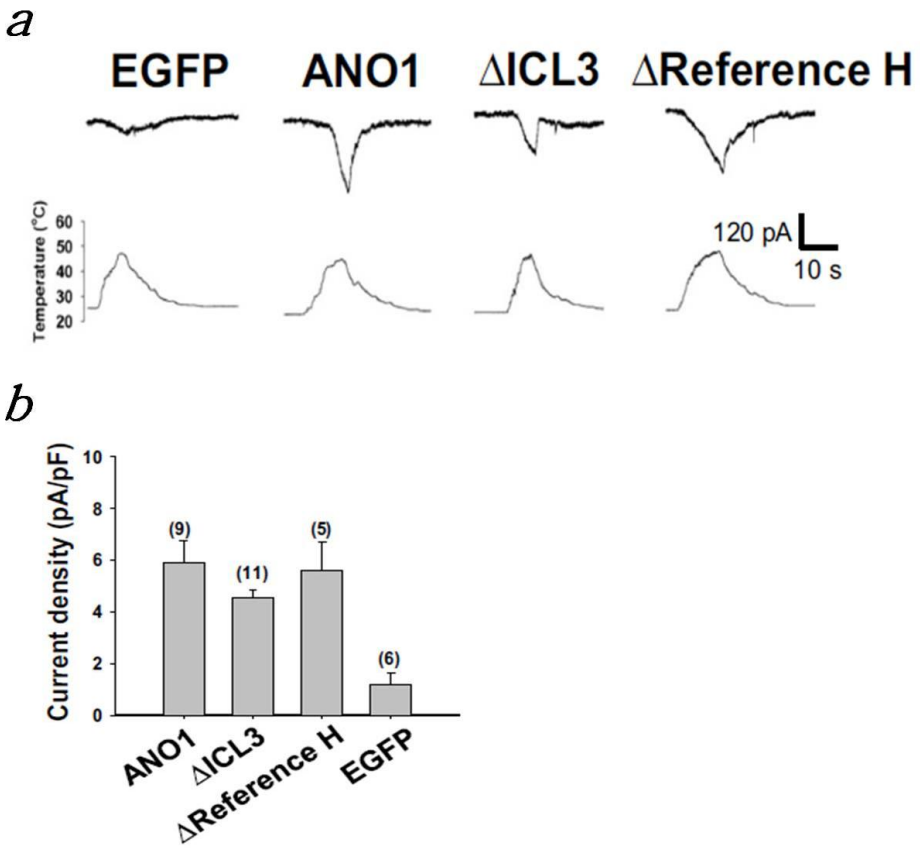

Figure 27. The two helices in the ICL3 region are dispensable for heat-induced ANO1 activation

(a) Traces of heat-induced whole cell currents of EGFP-, WT-, ΔICL3-, and Δreference helix mutant (Δ659-668)-transfected HEK293T cells. E_h=-60 mV. (b) A summary of heat-induced currents of ANO1 and its mutants.

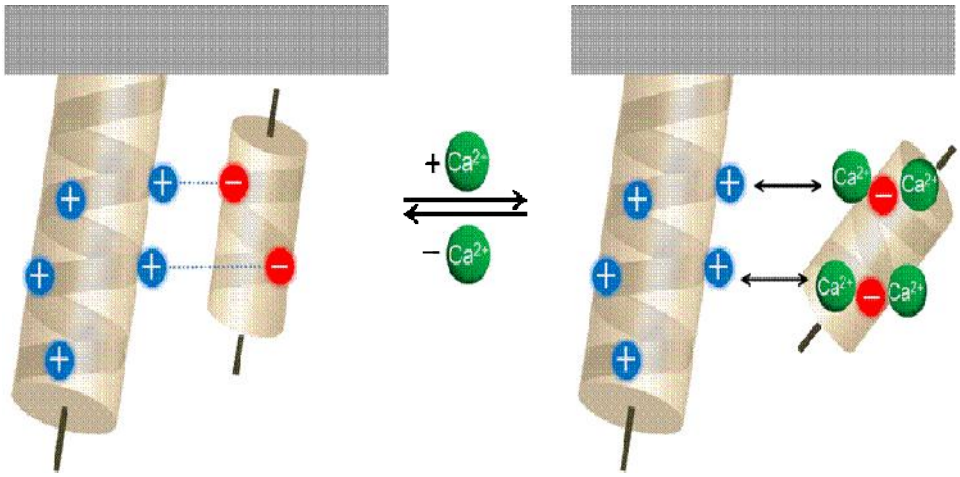

Figure 28. A schematic diagram depicting a molecular mechanism underlying Ca^{2+} -dependent activation of ANO1 at the ICL3 region

3.5 Comparison the structural prediction of the ICL3 region of ANO1/2 with the crystal structure of nectria haematococca TMEM16 (nhTMEM16)

In 2014, the first crystal structure of nhTMEM16, which belongs to TMEM16 family and serves as a lipid scramblase, was reported (Fig. 29a). The crystal structure consists of 10 transmembrane helices and contains highly conserved Ca^{2+} binding sites, such as E702 and E704 (Brunner et al., 2014). In additional, the structural properties of nhTMEM16A translated well for structure-function studies performed on TMEM16A because mutations at these sites right shift the dose response of Ca^{2+} (Brunner et al., 2014). Thus, to compare our predicted structures with the crystal structure, we again performed homologous modeling for ICL3 region of ANO1/2 based on the X-ray structure of nhTMEM16 (Fig. 29b). As our predicted structure of ICL3 of ANO2, the modeled structure of ICL3 of ANO2 based on the nhTMEM16 showed closely two parallel helices (Fig. 29b, c). However, in the modeled structure from nhTMEM16, the charged residues in two helices did not face each other. Also, the modeled Ca^{2+} sensor helix from the crystal structure embedded in the hydrophobic core of the membrane (Fig. 29b). These differences might result from a relatively low sequence identity between mouse ANO proteins and fungus ANO proteins. Furthermore, even the counterpart of the crystal structure of nhTMEM16 to

ICL3 of ANO2 represented a broken structure between reference helix and Ca^{2+} sensor helix as unstable structure. Therefore, the modeled structure based on crystal structure of nhTMEM16 might also work through the mechanism such as the conformational change of the two helix induced by Ca^{2+}.

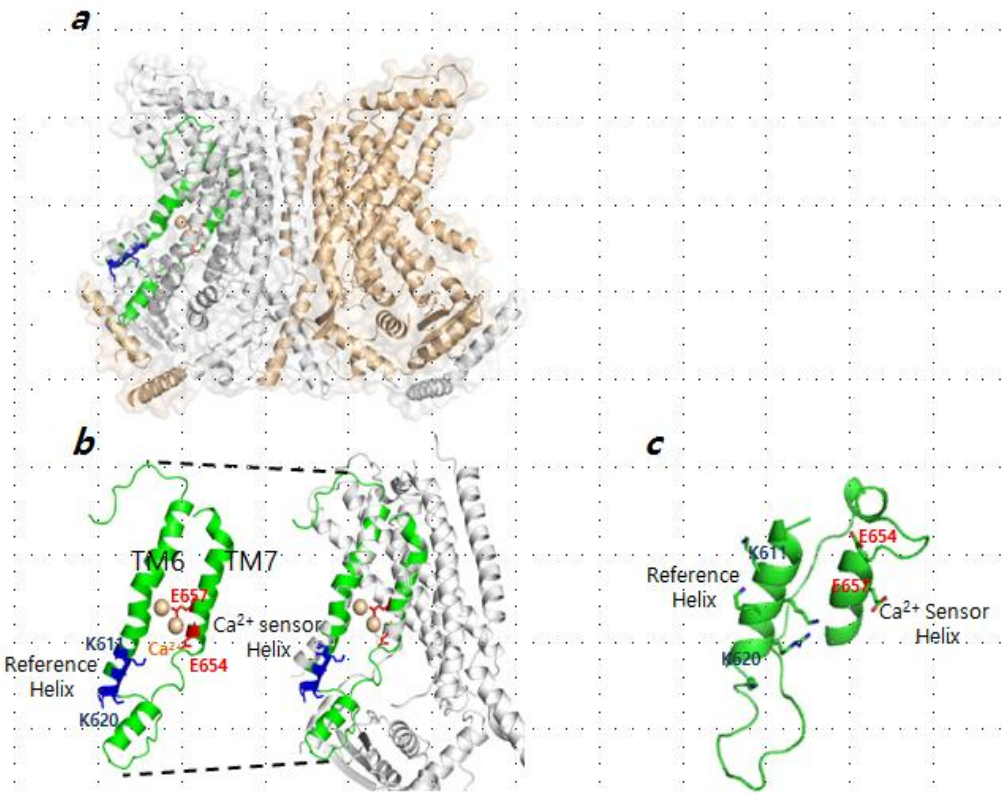

Figure 29. Comparison of predicted structure with the corresponding parts of the crystal structure nhTMEM16.

(a) Global structure of ICL3 of ANO2 based on nhTMEM16. (b) Enlarged view of the ICL3 of ANO2. Blue sticks represent positive residues in reference helix and red sticks represent negative residues in Ca2+ sensor helix, yellow ball represent bound Ca2+. (c) Homologous model of ICL3 of ANO2 based on partial H.pyroli.

Discussion

1. Ca^{2+}-binding site of ANO1

Since ANO1 was identified as CaCC, many studies tried to define the Ca^{2+} activation site in ANO1. Initially, the Ca^{2+} bowl-like region in the ICL1 was studied for the Ca2+ sensitivity (Xiao et al., 2011). However, the deletion of the region failed to show a shift in the Ca^{2+} sensitivity. Furthermore, Tien and colleagues observed that an "a" variant of ANO1 lacking the "EAVK" residues retains the EC50 of Ca^{2+} less than 1 μM, comparable to that of the "a,c" variant (Tien et al., 2014). Similarly, we also failed to see a discernible change in EC_{50} after the deletion of 444-EEEEE-448 (Fig. 14). In contrast, Xiao and Cui reported that the deletion of 444-EEEEEAVK-451 shifted ~40-fold increase in EC_{50} (Xiao et al., 2011). Yu and colleagues found the acidic residues, E702 and E705, in the ICL3 region of the revised topology that were critical for the Ca^{2+} sensitivity of ANO1 (Yu et al. 2012). Scudieri and colleagues also confirmed that this region is sensitive to the Ca2+-dependent activation (Scudieri et al. 2013). The present study also confirmed that this region is important for the ANO1 activation by Ca^{2+}. However, high Ca^{2+} also evoked currents in ΔICL3 mutant-expressing HEK cells. A possibility is that there are other multiple sites than the ICL3 region in ANO1 that controls the Ca^{2+}-dependent

activation. So, the deletion of the ICL3 region may not remove all the currents activated by Ca^{2+}. Recently, Tien and colleagues also suggest that the ICL3 region is an important site for the Ca^{2+} sensitivity (Tien et al., 2014). They extended mutation to E734 (equivalent to E730 in "a" variant) and D738 (equivalent to D734 in "a" variant) residues beyond the E702 and E705 residues and found that the E734 and D738 are involved in the Ca^{2+}-dependent gating, because mutations in these residues made a large shift in EC_{50} (Tien et al., 2014). Thus, Tien and colleagues proposed that the Ca^{2+} caging with the four Glu and Asp residues is essential for the ANO1 activation. Furthermore, the first crystal structure of nhTMEM16, which belongs to TMEM16 family and serves as a lipid scramblase, was reported (Fig 29a). In the crystal structure, two Ca^{2+} were bound by N650, E654, E702, E705, E734, and D738 which may form a novel Ca^{2+}-binding site (Brunner et al. 2014) including our ICL3 region.

2. Structural mechanism of activation by Ca^{2+} of ANO1

With homology modeling, we predicted that the ICL3 region in the revised topology of ANO1 has a unique structure composed of two parallel helices that interact with each other in a Ca^{2+}-dependent manner and cause rightward shifts in the Ca^{2+} sensitivity upon mutation. Furthermore, Eact, a synthetic agonist of ANO1, also acts on the ICL3 region. However, the two helices apparently did not control voltage-induced activation because

mutagenesis did not change the sensitivity to voltage. Furthermore, the ICL3 region did not account for heat-induced activation. This study was based on homology modeling, present experimental data including surface Plasmon resonance (SPR) assay, circular dichroism analysis, as well as mutational study along with electrophysiological experiments support the structure model. According to the model of ICL3 of ANO1, several structural elements appear important for the activation by Ca^{2+}. The two helices are oppositely charged. The role of positive charges in the reference helix appears to hold the Ca^{2+} sensor helix in the resting state. We imagine that the reference helix pushes the Ca^{2+}-sensor helix away when Ca^{2+} ions attach to it. Thus, removal of these positive charges in the reference helix decreases the direct binding and sensitivity to Ca^{2+} concentrations. However, because the removal of positive charges in the reference helix showed two-order differences in Ca^{2+} sensitivity that is smaller than the four-order change with the mutant in the Ca^{2+} sensor helix, other factors except for the ionic interaction between two helices may also contribute to the movement of two helices by Ca^{2+}. In line with this, positively charged amine residues of Lys and Arg in the reference helix do not align along one side facing the Ca^{2+} sensor helix. Instead, these positive charges distribute in many directions in a circular fashion. Furthermore, the other negative resides such as E654, E734, and D738 except for E702 and E705 appeared important for Ca2+ binding. However, it is not clear how Ca^{2+} binding to these sites gates

ANO1. It is conceivable that these additional negative residues except E702 and E705 may affect the interaction between Ca^{2+} and the reference Ca^{2+} sensor helices, because these each negative residue in three Ca^{2+} sensor helices are able to make Ca^{2+} binding to the region more stable than those in one Ca^{2+} sensor helix. When it come to these additional Ca^{2+} binding sites, it is conceivable that positive residues in reference helix might are also able to interact the other helices including E654, E734 and D738. Therefore, we have to identify whether the interactions between the other Ca^{2+} sensor helices and reference helix exist or not. In the case of ANO1's pore, the two papers present evidence that each subunit has its own distinct pore (Jeng et al., 2016; Lim et al., 2016). Furthermore, it has been known that TMEM16A heterodimerize with TMEM16B but not with TMEM16F (Whitlock and Hartzell, 2016). Therefore, the further structure studies relevant to Ca^{2+} binding should be considered to above structural characteristics.

3. Drug developmental implications

It has revealed that ANO1 play a role of a variety of cells, such as epithelial cells, nociceptive neuron, smooth muscle cells and cancer cells. Therefore, ANO1 pharmacological modulators may have broad therapeutic applications. For example, TMEM16A inhibitors may be useful in prevention of mucus hypersecretion, asthma, analgesia, anti-hypertension, and inhibition of cancer cell proliferation and migration (Fig. 30)

(Pedemonte and Galietta, 2014). By contrast, TMEM16A activators are able to have the potential ability to generate important side effects, such as bronchoconstriction, pain, and hypertension (Fig. 30) (Pedemonte and Galietta, 2014). Since ANO1 was discovered as a CaCC component, it was found that it is sensitive to the general Cl^- channel inhibitors (Fig. 31a), including niflumic acid, NPPB, DIDS, mefloquine, and fluoxetine in the 5–20 M range (Caputo A et al., 2008; Schroeder BC et al., 2008; Yang YD et al., 2008). The other ANO1 inhibitors, such as $CaCC_{inh}$-A01, $T16_{inh}A01$, benzbromarone, dichlorophen, and hexachlorophene, have been also identified by screening chemical libraries using a high-throughput functional assay (De La Fuente R et al, 2008; Namkung W et al., 2011; Huang F et al., 2012). Among these inhibitors, the compounds labeled $CaCC_{inh}$-A01 and $T16_{inh}A01$ have especially been used by different research groups to demonstrate the involvement of TMEM16A channel in a series of physiological and pathological processes including transepithelial ion transport, smooth muscle function, and cancer (Fig. 31b) (Davis AJ et al., 2013; Duvvuri U et al., 2012; Mroz MS et al., 2012; Sun H et al., 2012). Additionally, Natural compounds appeared as another interesting source of ANO1 inhibitor (Pedemonte and Galietta, 2014). For example, Tannic acids and other related compounds are an effective inhibitor of ANO1 currents and also have an inhibitory effect on the contractility of arterial smooth muscle (Namkung W et al., 2010) as well as MONNA which is anthranilic

acid derivative (Fig. 31c) (Oh SJ et al., 2013). In the case of ANO1 activator, E_{act} which is identified by screening chemical libraries using a high-throughput functional assay, could be useful as research tools and as potential drugs for the treatment of salivary gland dysfunction, cystic fibrosis, dry eye syndrome, intestinal hypomotility, and other disorders associated with Cl^- channel dysfunction (Fig. 31d) (Pedemonte and Galietta, 2014). However, it is not yet clear how these molecules act on ANO1. Moreover, several compounds have showed different result for roles of ANO1 when they were treated into the different cancer cells over-expressing ANO1. To find these problems, a better understanding of structural mechanism of activation by Ca^{2+} of ANO1 will be important for the rational development of selective drugs. Furthermore, two helices in ICL3 region might be important target region to develop the effective regulator of ANO1 based on tridimensional structure and its function.

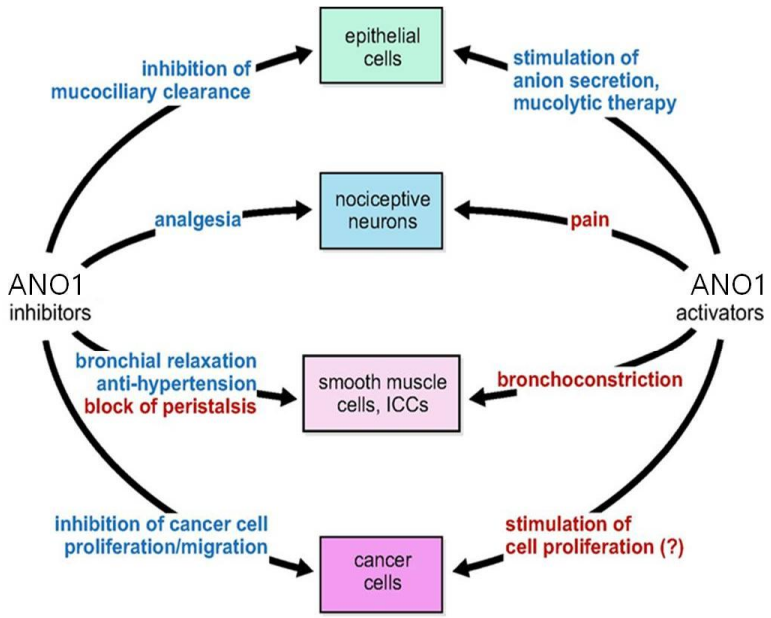

Pedemonte and Galietta, 2014, *Physiol Rev*

Figure 30. ANO1 as a drug target.

Scheme of possible pharmacological effects (blue: therapeutic effecs; red: potential undesired effects) of ANO1 activators and inhibitors. Stimulation of TMEM16A activity in the epithelial cells of the airways could potentially improve mucociliary clearance by enhancing the secretion of anions (Cl^- and bicarbonate) and the fluidification of mucus. However, because of ANO1 function in smooth muscle cells and nociceptive neurons, ANO1 activators could also cause bronchoconstriction and/or increased sensitivity to painful stimuli. Block of ANO1 function with inhibitors could be potentially beneficial to induce relaxation of smooth muscle cells in different organs (e.g., to treat hypertension). However, ANO1 inhibitors, by acting on ICCs, could also cause block of intestinal peristalsis.

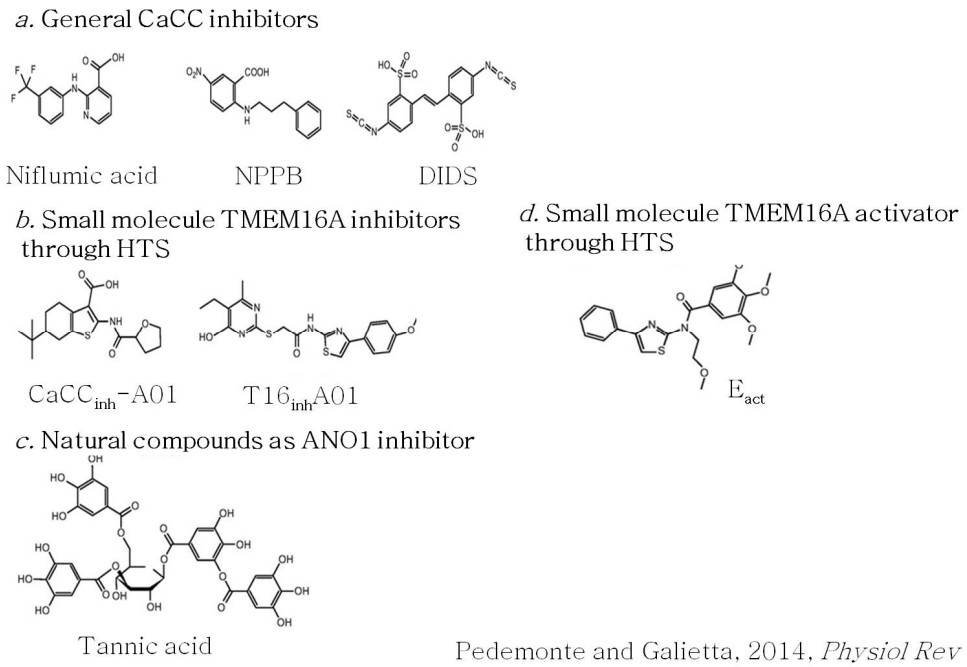

Figure 31. Pharmacological modulators of ANO1.

Structure of (a) general CaCC blockers (niflumic acid, NPPB, DIDS), of (b and c) new TMEM16A inhibitors ($T16_{inh}$-A01, $CaCC_{inh}$-A01, tannic acid), and of (d) a TMEM16A activator (E_{act}).

Reference

Almaca J, Tian Y, Aldehni F, Ousingsawat J, Kongsuphol P, Rock JR, Harfe BD, Schreiber R, Kunzelmann K (2009) TMEM16 proteins produce volume-regulated chloride currents that are reduced in mice lacking TMEM16A. J Biol Chem 284(42):28571-28578.

Andre S, Boukhaddaoui H, Campo B, Al Jumaily M, Mayeux V, et al (2003) Axotomy-induced expression of calcium activated chloride current in subpopulations of mouse dorsal root ganglion neurons. *J. Neurophysiol.* 90:3764–73.

Arreola J, Melvin JE, Begenisich T (1995) Inhibition of Ca^{2+}-dependent Cl^- channels from secretory epithelial cells by low internal pH. *J. Membr. Biol.* 147:95–104.

Arreola J, Melvin J, Begenisich T (1996) Activation of calcium-dependent chloride channels in rat paroid acinar cells. *J. Gen.Physiol.* 108:35–47

Arreola J, Melvin JE, Begenisich T (1998) Differences in regulation of Ca^{2+}-activated Cl^- channels in colonic and parotid secretory cells. *Am. J. Physiol.Cell Physiol.* 274:C161–66.

Arreola J, Begenisich T, Nehrke K, Nguyen HV, Park K, Richardson L, Yang B, Schutte BC, Lamb FS, Melvin JE (2002) Secretion and cell volume regulation by salivary acinar cells from mice lacking expression of the Clcn3 Cl− channel gene. *J Physiol* 545: 207-216.

Bader CR, Bertrand D, Schlichter R (1987) Calcium-activated chloride current in cultured sensory and parasympathetic quail neurones. *J. Physiol.* 394:125–48.

Barrett KE, Keely SJ (2000) Chloride secretion by the intestinal epithelium: molecular basis and regulatory aspects. *Annu. Rev. Physiol.* 62:535–72.

Barro-Soria R, Aldehni F, Almac¸a J, Witzgall R, Schreiber R, Kunzelmann K (2010) ER-localized bestrophin 1 activates Ca2+-dependent ion channels TMEM16A and SK4 possibly by acting as a counterion channel. *Pfl¨ugers Arch* 459: 485-497.

Begenisich T, Melvin JE (1998) Regulation of chloride channels in secretory epithelia. *J. Membr. Biol.* 163:77–85.

Bian S, Favre I & Moczydlowski E (2001) Ca2+-binding activity of a COOH-terminal fragment of the Drosophila BK channel involved in Ca2+-dependent activation. *Proc Natl Acad Sci U S A* 98, 4776-4781.

Billig GM, Pal B, Fidzinski P, Jentsch TJ (2011) Ca^{2+}-activated Cl- currents are dispensable for olfaction. Nature Neuroscience 14:763-769.

Byrne NG, LargeWA. (1987) Action of noradrenaline on single smooth muscle cells freshly dispersed from the rat anococcygeus muscle. *J Physiol* 389:513-525.

Botelho SY, Dartt DA (1980) Effect of calcium antagonism or chelation on rabbit lacrimal gland secretion and membrane potentials. *J. Physiol.* 304:397–403.

Boucher RC, Cheng EHC, Paradiso AM, Stutts MJ, Knowles MR, Earp HS. (1989) Chloride secretory response of cystic fibrosis human airway epithelia: preservation of calcium but not protein kinase C- and A-dependent mechanisms. *J. Clin.Invest.* 84:1424–31.

Brunner JD, Lim NK, Schenck S, Duerst A, Dutzler R (2014) X-ray structure of a calcium-activated TMEM16 lipid scramblase. Nature 516:207–212

Caputo A, Caci E, Ferrera L, Pedemonte N, Barsanti C, Sondo E, Pfeffer U, Ravazzolo R, Zegarra-Moran O, Galietta LJ (2008) TMEM16A, a membrane protein associated with calcium-dependent chloride channel activity. *Science* 322: 590-594.

Carles, A., R. Millon, A. Cromer, G. Ganguli, F. Lemaire, J. Young, et al. (2006) Head and neck squamous cell carcinoma transcriptome analysis by comprehensive validated differential display. Oncogene 25:1821–1831.

Carneiro, A., A. Isinger, A. Karlsson, J. Johansson, G. Jonsson, P. O. Bendahl, et al. 2008. Prognostic impact of array-based genomic profiles in esophageal squamous cell cancer. BMC Cancer 8:98.

Cha JY, Wee J, Jung J, Jang Y, Lee B, Hong GS, Chang BC, Choi YL, Shin YK, Min HY, Lee HY, Na TY, Lee MO, Oh U (2015) Anoctamin 1 (TMEM16A) is essential for testosterone-induced prostate hyerplasia. Proc Natl Acad Sci USA;112:9722–9727

Chan HC, Kaetzel MA, Gotter AL, Dedman JR, Nelson DJ (1994) Annexin IV inhibits calmodulin-dependent protein kinase II-activated chloride conductance: a novel mechanism for ion channel regulation. *J. Biol. Chem.* 269(51):32464–68.

Chao AC, Kouyama K, Heist EK, Dong YJ, Gardner P (1995) Calciumand CaMKII-dependent chloride secretion induced by the microsomal Ca2+-ATPase inhibitor 2,5-di-(tert-butyl)-1,4-hydroquinone in cystic fibrosis pancreatic epithelial cells. *J. Clin. Invest.* 96:1794–801.

Cho H, Yang YD, Lee J, Lee B, Kim T, Jang Y, Back SK, Na HS, Harfe BD, Wang F, Raouf R, Wood JN, Oh U (2012) The calcium-activated chloride channel anoctamin 1 acts as a heat sensor in nociceptive neurons. Nat Neurosci 15(7):1015-1021.

Collier ML, Levesque PC, Kenyon JL, Hume JR (1996) Unitary Cl− channels activated by cytoplasmic Ca2+ in canine ventricular myocytes. *Circ. Res.* 78:936–44.

Contreras-Vite JA, Cruz-Rangel S, De Jesus-Perez JJ, Figueroa IA, Rodriguez-Menchaca AA, Perez-Cornejo P, Hartzell HC, Arreola J. 2016. Revealing the activation pathway for TMEM16A chloride

channels from macroscopic currents and kinetic models. Pflugers Arch 468(7):1241-1257.

Crain SM (1956) Resting and action potentials of cultured chick embryo spinal ganglion cells. *J. Comp. Neurol.* 104:285–329.

Cruz-Rangel S, De Jesus-Perez JJ, Contreras-Vite JA, Perez-Cornejo P, Hartzell HC, Arreola J (2015) Gating modes of calcium-activated chloride channels TMEM16A and TMEM16B. J Physiol 593(24):5283-5298.

Currie KP, Wootton JF, Scott RH (1995) Activation of Ca2+-dependent Cl− currents in cultured rat sensory neurones by flash photolysis of DM-nitrophen. *J.Physiol.* 482(Pt. 2):291–307.

Das S, Hahn Y, Walker DA, Nagata S, Willingham MC, Peehl DM, Bera TK, Lee B, Pastan I (2008) Topology of NGEP, a prostate-specific cell:cell junction protein widely expressed in many cancers of different grade level. Cancer Res 68(15):6306-6312.

Davis AJ, Forrest AS, Jepps TA, Valencik ML, Wiwchar M, Singer CA, Sones WR, Greenwood IA, and Leblanc N (2010) Expression profile and protein translation of TMEM16A in murine smooth muscle. *Am J Physiol Cell Physiol* **299:**C948–C959.

Davis AJ, Shi J, Pritchard HA, Chadha PS, Leblanc N, Vasilikostas G, Yao Z, Verkman A, Albert AP, Greenwood IA (2013) Potent vasorelaxant activity of the TMEM16A inhibitor T16Ainh-A01. Br J Pharmacol 168: 773–784.

De Castro F, Geijo-Barrientos E, Gallego R (1997) Calcium-activated chloride current in normal mouse sympathetic ganglion cells. *J. Physiol.* 498(Part 2):397–408

De La Fuente R, Namkung W, Mills A, Verkman AS (2008) Small-molecule screen identifies inhibitors of a human intestinal calcium-activated chloride channel. Mol Pharmacol 73: 758 –768.

Deschenes M, Feltz P, Lamour Y (1976) A model for an estimate in vivo of the ionic basis of presynaptic inhibition: an intracellular analysis of the GABA-induced depolarization in rat dorsal root ganglia. *Brain Res.* 118:486–93

Dho S, Stewart K, Foskett JK (1992) Purinergic receptor activation of Cl− secretion in T84 cells. *Am. J. Physiol. Cell Physiol.* 262:C67–74

Douglas WW, Poisner AM (1963) The influence of calcium on the secretory response of the submaxillary gland to acetylcholine or to noradrenaline. *J. Physiol.*165:528–41

Duchen MR (1990) Effects of metabolic inhibition on the membrane properties of isolated mouse primary sensory neurones. *J. Physiol.* 424:387–409

Duran C, C Hartzell (2011) Physiological roles and diseases of tmem16/anoctamini proteins: are they all chloride channels? Acta Pharmacological Sinica 31:685-692

Duran C, Qu Z, Osunkoya AO, Cui Y, Hartzell HC (2012) ANOs 3-7 in the anoctamin/Tmem16 Cl- channel family are intracellular proteins. Am J Physiol Cell Physiol 302:C482–C493

Duvvuri U, Shiwarski DJ, Xiao D, Bertrand C, Huang X, Edinger RS, Rock JR, Harfe BD, Henson BJ, Kunzelmann K, Schreiber R, Seethala RS, Egloff AM, Chen X, Lui VW, Grandis JR, Gollin SM (2012) TMEM16A induces MAPK and contributes directly to tumorigenesis and cancer progression. Cancer Res 72: 3270 –3281.

Eggermont J (2004) Calcium-activated chloride channels: (un)known, (un)loved? *Proc Am Thorac Soc* 1: 22-27.

Evans MG, Marty A (1986) Calcium dependent chloride currents in isolated cells from rat lacrimal glands. *J. Physiol.*378:437–60

Fallah G, Romer T, Detro-Dassen S, Braam U, Markwardt F, Schmalzing G (2011) TMEM16A(a)/anoctamin-1 shares a homodimeric architecture with CLC chloride channels. Mol Cell Proteomics 10(2):M110 004697.

Ferrera L, Zegarra-Moran O, J.V. Galietta (2011) Ca^{2+}-Activated Cl^- Channels. Compr Physiol 1:2155-2174.

Ferrer-Montiel AV, Merino JM, Blondelle SE, Perez-Paya E, Houghten RA and Motal M (1998) Selected peptides targeted to the NMDA receptor channel protect neurons from excitotoxic death. *Nat. Biotechnol* DOI:10.1038/nbt0398-286

Flores CA, Cid LP, Sepu´ lveda FV, and Niemeyer MI (2009) TMEM16 proteins: the long awaited calcium-activated chloride channels? *Braz J Med Biol Res* **42:**993–1001.

Frings S, Reuter D, Kleene SJ (2000) Neuronal Ca^{2+} -activated Cl^- channels--homing in on an elusive channel species. Prog Neurobiol. Feb;60(3):247-89.

Galietta LJV (2009) The TMEM16 protein family : a new class of chloride channels? Biophys 97(12):3047-3053.

Gifford JL, Walsh MP & Vogel HJ (2007) Structures and metal-ion-binding properties of the Ca2+-binding helix-loop-helix EF-hand motifs. *Biochem J* 405, 199-221.

Giovannucci DR, Bruce JI, Straub SV, Arreola J, Sneyd J, et al (2002) Cytosolic Ca^{2+} and Ca^{2+}-activated Cl^- current dynamics: insights from two functionally distinct mouse exocrine cells. *J. Physiol.* 540:469–84

Gomez-Pinilla PJ, Gibbons SJ, Bardsley MR, Lorincz A, Pozo MJ, Pasricha PJ, Van de Rijn M, West RB, Sarr MG, Kendrick ML, et al. (2009) Ano1 is a selective marker of interstitial cells of Cajal in the human

and mouse gastrointestinal tract. *Am J Physiol Gastrointest Liver Physiol* **296:**G1370–G1381.

Gritli-Linde A, Vaziri Sani F, Rock JR, Hallberg K, Iribarne D, Harfe BD, and Linde A (2009) Expression patterns of the Tmem16 gene family during cephalic development in the mouse. *Gene Expr Patterns* **9:**178–191.

Grubb S, Poulsen KA, Juul CA, Kyed T, Klausen TK, Larsen EH, Hoffmann EK (2013) TMEM16F (Anoctamin 6), an anion channel of delayed Ca_2 activation. *J Gen Physiol* 141: 585–600.

Hallani M, Lynch JW, Barry PH (1998) Characterization of calcium-activated chloride channels in patches excised from the dendritic knob of mammalian olfactory receptor neurons. *J Membr Biol* 161: 163-171.

Hartzell HC (1996) Activation of different Cl currents in *Xenopus* oocytes by Ca liberated from stores and by capacitative Ca influx. *J. Gen. Physiol.* 108:157–75

Hartzell HC, Putzier I, Arreola J (2005) Calcium-activated chloride channels. Annu Rev Physiol 67:719-758.

Hartzell HC, Qu Z, Yu K, Xiao Q, Chien LT (2008) Molecular physiology of bestrophins: Multifunctional membrane proteins linked to best disease and other retinopathies. *Physiol Rev* 88: 639-672.

Holevinsky KO, Jow F, Nelson DJ (1994) Elevation in intracellular calcium activates both chloride and proton currents in human macrophages. *J. Membr. Biol.*140:13–30

Huang F, Rock JR, Harfe BD, Cheng T, Huang X, Jan YN, and Jan LY (2009) Studies on expression and function of the TMEM16A calcium-activated chloride channel. *Proc Natl Acad Sci USA* **106:**21413–21418.

Huang F, Zhang H, Wu M, Yang H, Kudo M, Peters CJ, Woodruff PG, Solberg OD, Donne ML, Huang X, Sheppard D, Fahy JV, Wolters PJ, Hogan BL, Finkbeiner WE, Li M, Jan YN, Jan LY, Rock JR (2012) Calcium-activated chloride channel TMEM16A modulates mucin secretion and airway smooth muscle contraction. Proc Natl Acad Sci USA 109: 16354 –16359.

Huang F, Wong X, Lily Y. Jan (2012) International Union of Basic and Clinical Pharmcology. LXXXV: Cacium-Activated Chloride Channels. Pharmacol Rev. 64(1):1-15.

Huang F, Wang X, Ostertag EM, Nuwal T, Huang B, Jan YN, Basbaum AI, Jan LY (2013) TMEM16C facilitates Na^+-activated K^+ currents in rat sensory neurons and regulates pain processing. *Nat Neurosci* 16: 1284–1290.

Huang P, Liu J, Di A, Robinson NC, Musch MW, Kaetzel MA, Nelson DJ (2001) Regulation of human CLC-3 channels by multifunctional

Ca2+/calmodulin-dependent protein kinase. *J Biol Chem* 276: 20093-20100.

Huang WC, Xiao S, Huang F, Harfe BD, Jan YN, Jan LY (2012) Caclium-activated chloride channels (CaCCs) regulate action potential and synaptic response in hippocampal neurons. Neuron 74:179-192.

Hunter M, Smith PA, Case RM (1983) The dependence of fluid secretion by mandibular salivary gland and pancreas on extracellular calcium. *Cell Calcium* 4:307–17

Hwang SJ, Blair PJ, Britton FC, O'Driscoll KE, Hennig G, Bayguinov YR, Rock JR, Harfe BD, Sanders KM, and Ward SM (2009) Expression of anoctamin 1/TMEM16A by interstitial cells of Cajal is fundamental for slow wave activity in gastrointestinal muscles. *J Physiol* **587:**4887–4904.

Jentsch TJ, Stein V, Weinreich F, Zdebik AA (2002) Molecular structure and physiological function of chloride channels. *Physiol Rev* 82: 503-568.

Jeng G, Aggarwal M, Yu WP, and Chen TY. (2016) Independent activation of distinct pores in the dimeric TMEM16A channels. *J. Gen. Physiol.* 148. http ://dx .doi .org /10 .1085 /jgp .201611651

Kachintorn U, Vajanaphanich M, Traynor-Kaplan AE, Dharmsathaphorn K, Barrett KE (1993) Activation by calcium alone of chloride secretion in T84 epithelial cells. *Br. J. Pharmacol.* 109:510–17

Kaetzel MA, Pula G, Campos B, Uhrin P,Horseman N, Dedman JR (1994) A role for annexin IV in epithelial cell function.Inhibition of calcium-activated chloride conductance. *J. Biol. Chem.* 269:5297–302

Kaneko H, Putzier I, Frings S, Gensch T (2002) Determination of intracellular chloride concentration in dorsal root ganglion neurons by fluorescent lifetime imaging. CURR TOP MEMBR. 167–89

Kartner N, Hanrahan JW, Jensen TJ, Naismith AL, Sun SZ, et al. 1991. Expression of the cystic fibrosis gene in non-epithelial invertebrate cells produces a regulated anion conductance. *Cell* 64:681–91

Katoh, M., and M. Katoh. 2003. FLJ10261 gene, located within the CCND1-EMS1 locus on human chromosome 11q13, encodes the eight-transmembrane protein homologous to C12orf3, C11orf25 and LJ34272 gene products. Int. J. Oncol. 22:1375–1381.

Kimelberg HK et al. (2000) Active accumulation and exchange transport of chloride in astroglial cells in culture. Biochim Biophys Acta 646: 179-184, 1981

Kleene SJ, Gesteland RC (1991) Calcium-activated chloride conductance in frog olfactory cilia. *J Neurosci* 11: 3624-3629.

Kleene SJ (1997) High-gain, low-noise amplification in olfactory transduction. *Biophys. J.* 73:1110–17

Kmit A, van Kruchten R, Ousingsawat J, Mattheij NJ, Senden-Gijsbers B, Heemskerk JW, Schreiber R, Bevers EM, Kunzelmann K (2013) Calcium-activated and apoptotic phopholipid scrambling induced by Ano6 can occur independently of Ano6 ion currents. Cell Death & Disease 4:e611.

Knowles MR, Clarke LL, Boucher RC (1991) Activation by extracellular nucleotides of chloride secretion in the airway epithelia of patients with cystic fibrosis. *N. Engl. J. Med.* 325:533–38

Koumi S, Sato R, Aramaki T (1994) Characterization of the calcium-activated chloride channel in isolated guinea-pig hepatocytes. *J. Gen. Physiol.* 104:357–73

Kuruma A, Hartzell HC (2000) Bimodal control of a Ca2+ -activated Cl− channel by different Ca2+ signals. *J. Gen. Physiol* .115:59–80

Large WA and Wang Q (1996) Characteristics and physiological role of the Ca^{2+}-activated Cl^- conductance in smooth muscle. *Am J Physiol* **271:**C435–C454.

Ling BN, Seal EE, Eaton DC (1993) Regulation of mesangial cell ion channels by insulin and angiotensin II. Possible role in diabetic glomerular hyperfiltration. *J.Clin. Invest.* 92:2141–51

Lowe G, Gold GH (1993) Contribution of the ciliary cyclic nucleotide-gated conductance to olfactory transduction in the salamander. *J. Physiol.* 462:175–96

Lee RJ and Foskett JK (2010) Mechanisms of Ca^{2+}-stimulated fluid secretion by porcine bronchial submucosal gland serous acinar cells. *Am J Physiol Lung Cell Mol Physiol* **298:**L210–L231.

Lim NK, AKM Lam, and R.Dutzler (2016) Independent activation of ion conduction pores in the double-barreled calcium-activated chloride channel TMEM16A. *J. Gen. Physiol.* 148. http://dx .doi .org /10 .1085 /jgp .201611650

Liu B, Linley JE, Du X, Zhang X, Ooi L, Zhang H, Gamper N (2010) The acute nociceptive signals induced by bradykinin in rat sensory neurons are mediated by inhibition of M-type K+ channels and activation of Ca2+-activated Cl− channels. *J Clin Invest* 120: 1240-1252.

Ma K, Wang H, Yu J, Wei M, Xiao Q (2016) New insights on the regulation of Ca^{2+}-activated chloride channel TMEM16A. *J Cell Physiol* DOI 10.1002/jcp.25621

Manoury B, Tamuleviciute A, Tammaro P (2010) TMEM16A/anoctamin 1 protein mediates calcium-activated chloride currents in pulmonary arterial smooth muscle cells. J Physiol 588(Pt 13):2305-2314.

Marmorstein LY, Wu J, McLaughlin P, Yocom J, Karl MO, Neussert R, Wimmers S, Stanton JB, Gregg RG, Strauss O, Peachey NS, Marmorstein AD (2006) The light peak of the electroretinogram is

dependent on voltage-gated calcium channels and antagonized by bestrophin (Best-1). *J Gen Physiol* 127: 577-589.

Martins JR, Faria D, Kongsuphol P, Reisch B, Schreiber R, Kunzelmann K (2011) Anoctamin 6 is an essential component of the outwardly rectifying chloride channel. *Proc Natl Acad Sci USA* 108: 18168–18172.

Matchkov VV, Aalkjaer C, Nilsson H (2004) A cyclic GMP-dependent calcium activated chloride current in smooth muscle cells from rat mesenteric resistance arteries. *J. Gen. Physiol.* 123:121–34

Matsuda JJ, Filali MS, Collins MM, Volk KA, Lamb FS (2010) The ClC-3 Cl−/H+ antiporter becomes uncoupled at low extracellular pH. *J Biol Chem* 285: 2569-2579.

Martin DK (1993) Small conductance chloride channels in acinar cells from the rat mandibular salivary gland are directly controlled by a G-protein. *Biochem. Biophys. Res. Commun.* 192:1266–73

Mayer ML. 1985. A calcium-activated chloride current generates the afterdepolarization of rat sensory neurones in culture. *J. Physiol.* 364:217–39

Manoury B, Tamuleviciute A, and Tammaro P (2010) TMEM16A/anoctamin 1 protein mediates calcium-activated chloride currents in pulmonary arterial smooth muscle cells. *J Physiol* **588:**2305–2314.

Melvin JE, Koek L, Zhang GH (1991) A capacitative Ca2+ influx is required for sustained fluid secretion in sublingual mucous acini. *Am. J. Physiol. Gastrointest. Liver Physiol.* 261:G1043–50

Melvin JE, Yule D, Shuttleworth TJ, Begenisich T (2005) Regulation of fluid and electrolyte secretion in salivary gland cells. *Annu. Rev. Physiol.* 67:445–69

Mroz MS, Keely SJ (2012) Epidermal growth factor chronically upregulates Ca2-dependent Cl conductance and TMEM16A expression in intestinal epithelial cells. J Physiol 590: 1907–1920.

Namkung W, Thiagarajah JR, Phuan PW, Verkman AS (2010) Inhibition of Ca^{2+}-activated Cl channels by gallotannins as a possible molecular basis for health benefits of red wine and green tea. FASEB J 24: 4178 – 4186.

Namkung W, Yao Z, Finkbeiner WE, Verkman AS (2011) Small-molecule activators of TMEM16A, a calcium-activated chloride channel, stimulate epithelial chloride secretion and intestinal contraction. FASEB J 25(11):4048-4062

Nishimoto I, Wagner J, Schulman H, Gardner P (1991) Regulation of Cl− channels by multifunctional CaM kinase. *Neuron* 6:547–55

Nilius B, Prenen J, Szucs G,Wei L, Tanzi F, et al (1997) Calcium-activated chloride channels in bovine pulmonary artery endothelial cells. *J. Physiol.* 498:381–96

Nilius B, Prenen J, Voets T, Van Den Bremt K , Eggermont J, Droogmans G (1997) Kinetic and pharmacological properties of the calcium-activated chloride-current in microvascular endothelial cells. *Cell Calcium* 22:53–63

Oh SJ, Hwang SJ, Jung J, Yu K, Kim J, Choi JY, Hartzell HC, Roh EJ, Lee CJ (2013) MONNA, a potent and selective blocker for transmembrane protein with unknown function 16/anoctamin-1. Mol Pharmacol 84: 726 –735.

Okada T, Horiguchi H, Tachibana M (1995) Ca^{2+}-dependent Cl^- current at the presynaptic terminals of goldfish retinal bipolar cells. *Neurosci. Res.* 23:297–303

Ousingsawat J, Martins JR, Schreiber R, Rock JR, Harfe BD, Kunzelmann K (2009) Loss of TMEM16A causes a defect in epithelial Ca2+-dependent chloride transport. *J Biol Chem* 284: 28698-28703.

Park K, Brown PD (1995) Intracellular pH modulates the activity of chloride channels in isolated lacrimal gland acinar cells. *Am. J. Physiol. Cell Physiol.* 268:C647–50.

Park MK, Lomax RB, Tepikin AV, Petersen OH (2001) Local uncaging of caged Ca2+-activated Cl− channels in pancreatic acinar cells. *Proc. Natl. Acad. Sci. USA* 98:10948–53.

Patel AC, Brett TJ, Holtzman MJ (2009) The role of CLCA proteins in inflammatory airway disease. *Annu Rev Physiol* 71: 425-449.

Pacaud P, Loirand G, Mironneau C, Mironneau J. (1989) Noradrenaline activates a calcium-activated chloride conductance and increases the voltage-dependent calcium current in cultured single cells of rat portal vein. *Br J Pharmacol* 97: 139-146.

Pedemonte N, Galietta LJV (2104) STRUCTURE AND FUNCTION OF TMEM16 PROTEINS (ANOCTAMINS). *Physiol Rev* 94: 419–459.

Petrukhin K, Koisti MJ, Bakall B, Li W, Xie G, Marknell T, Sandgren O, Forsman K, Holmgren G, Andreasson S, Vujic M, Bergen AAB, McGarty-Dugan V, Figueroa D, Austin CP, Metzker ML, Caskey CT, Wadelius C (1998) Identification of the gene responsible for Best macular dystrophy. *Nature Genet* 19: 241-247.

Pifferi S, Dibattista M, and Menini A (2009) TMEM16B induces chloride currents activated by calcium in mammalian cells. *Pflugers Arch* **458:**1023–1038.

Piper AS, LargeWA (2003) Multiple conductance states of single Ca^{2+}-activated Cl^- channels in rabbit pulmonary artery smooth muscle cells. *J. Physiol.* 547:181–96.

Piper AS, LargeWA (2004) Single cGMP activated Ca^{2+}-dependent Cl^- channels in rat mesenteric artery smooth muscle cells. *J. Physiol.* 555:397–408.

Pietra G, Dibattista M, Menini A, Reisert J, Boccaccio A (2016) The Ca2+-activated Cl-channel TMEM16B regulates action potential firing and

axonal targeting in olfactory sensory neurons. J Gen Physiol 148(4):293-311.

Planells-Cases R, Aracil A, Merino JM, Gallar J, Perez-paya E, Belmonte C, Gonzalez-Ros JM and Ferrer-Montiel AV (2000) Arginine-rich peptides are blockers of VR-1 channels with analgesic activity, *FEBS Lett* **DOI:** 10.1016/S0014-5793(00)01982-7

Qu Z, Fischmeister R, Hartzell C (2004) Mouse bestrophin-2 is a bona fide Cl− channel: Identification of a residue important in anion binding and conduction. *J Gen Physiol* 123: 327-340.

Rasche S, Toetter B, Adler J, Tschapek A, Doerner JF, Kurtenbach S, Hatt H, Meyer H, Warscheid B, and Neuhaus EM (2010) Tmem16b is specifically expressed in the cilia of olfactory sensory neurons. *Chem Senses* **35:**239–245.

Reisert J, Bauer PJ, Yau KW, Frings S (2003) The Ca-activated Cl channel and its control in rat olfactory receptor neurons. *J. Gen. Physiol.* 122:349–64.

Rock JR, O'Neal WK, Gabriel SE, Randell SH, Harfe BD, Boucher RC, Grubb BR (2009) Transmembrane protein 16A (TMEM16A) is a Ca2+-regulated Cl− secretory channel in mouse airways. *J Biol Chem* 284:14875-14880.

Romanenko VG, Catal´an MA, Brown DA, Putzier I, Hartzell HC, Marmorstein AD, Gonzalez-Begne M, Rock JR, Harfe BD, Melvin JE (2010) Tmem16A encodes the Ca2+-activated Cl− channel in mouse submandibular salivary gland acinar cells. *J Biol Chem*285: 12990-13001.

Sagheddu C, Boccaccio A, Dibattista M, Montani G, Tirindelli R, and Menini A (2010) Calcium concentration jumps reveal dynamic ion selectivity of calcium-activated chloride currents in mouse olfactory sensory neurons and TMEM16b-transfected HEK 293T cells. *J Physiol* **588:**4189–4204.

Saleh SN, Greenwood IA. (2005) Activation of chloride currents in murine portal vein smooth muscle cells by membrane depolarization involves intracellular calcium release. *Am J Physiol* 288: C122-C131.

Sa´nchez-Vives, M. V. and Gallego, R (1994) Calciumdependent chloride current induced by axotomy in rat sympathetic neurons. J. Physiol. Lond. 475, 391-400.

Schlenker T, Fitz JG (1996) Ca2+-activated Cl− channels in human biliary cell line: regulation by Ca2+/calmodulindependent protein kinase. *Am. J. Physiol.Gastrointest. Liver Physiol.* 271:G304–10

Schreiber R, Uliyakina I, Kongsuphol P, Warth R, Mirza M, Martins JR, Kunzelmann K (2010) Expression and function of epithelial anoctamins. *J Biol Chem* 285: 7838–7845, 2010.

Schroeder BC, Cheng T, Jan YN, Jan LY (2008) Expression cloning of TMEM16A as a calcium-activated chloride channel subunit. *Cell* 134: 1019-1029.

Schild D, Restrepo D (1998) Transduction mechanisms in vertebrate olfactory receptor cells. *Physiol. Rev.* 78:429–66

Scott RH, McGuirk SM, Dolphin AC (1988) Modulation of divalent cationactivated chloride ion currents. *Br. J.Pharmacol.* 94:653–62

Sucdieri P, Sondo E, Caci E, Ravazzolo R, Galietta LJ (2013) TMEM16A-TMEM16B chimeras to investigate the structurefunction relationship of calcium-activated chloride channels. Biochem J 452(3):443

Sheridan JT, Worthington EN, Yu K, Gabriel SE, Hartzell HC, Tarran R (2011) Characterization of the oligomeric structure of the Ca(2+)-activated Cl- channel Ano1/TMEM16A. J Biol Chem 286(2):1381-1388.

Shimizu T, Iehara T, Sato K, Fujii T, Sakai H, Okada Y (2013) TMEM16F is a component of a Ca^{2+}-activated Cl^- channel but not a volume-sensitive outwardly rectifying Cl_ channel. *Am J Physiol Cell Physiol* 304: C748–C759.

Stapleton SR, Scott RH, Bell BA (1994) Effects of metabolic blockers on Ca2+-dependent currents in cultured sensory neurones from neonatal rats. *Br. J. Pharmacol.*111:57–64

Sto¨hr H, Heisig JB, Benz PM, Scho¨berl S, Milenkovic VM, Strauss O, Aartsen WM, Wijnholds J, Weber BH, and Schulz HL (2009) TMEM16B, a novel protein with calcium-dependent chloride channel activity, associates with a presynaptic protein complex in photoreceptor terminals. *J Neurosci* **29:**6809–6818.

Sung, K., Kirby, M. and McDonald, M (2000) Abnormal GABAA receptor-mediated currents in dorsal root ganglion neurons isolated from Na-K-2Cl cotransporter null mice. J. Neurosci. 20, 7531-7538.

Sun H, Xia Y, Paudel O, Yang XR, Sham JS (2012) Chronic hypoxia-induced upregulation of Ca2-activated Cl channel in pulmonary arterial myocytes: a mechanism contributing to enhanced vasoreactivity. J Physiol 590: 3507–3521.

Suzuki J, Umeda M, Sims PJ, Nagata S (2010) Calcium-dependent phospholipid scrambling by TMEM16F. Nature 468:834-838.

Suzuki J, Fujii T, Imao T, Ishihara K, Kuba H, Nagata S (2013) Calcium-dependent phospholipid scramblase activity of TMEM16 protein family members. *J Biol Chem* 288: 13305–13316.

Tarran R, Loewen ME, Paradiso AM, Olsen JC, Gray MA, et al (2002) Regulation of murine airway surface liquid volume by CFTR and Ca2+-activated Cl− conductances. *J. Gen. Physiol.* 120:407 18

Terashima H, Picollo A, Accardi A. 2013. Purified TMEM16A is sufficient to form Ca^{2+}-activated Cl- channels. Proc Natl Acad Sci U S A 110(48):19354-19359.

Thomas-Gatewood C, Neeb ZP, Bulley S, Adebiyi A, Bannister JP, Leo MD, Jaggar JH (2011) TMEM16A channels generate Ca(2)(+)-activated Cl(-) currents in cerebral artery smooth muscle cells. Am J Physiol Heart Circ Physiol 301(5):H1819-1827.

Tian Y, Scheriber R, Kunzelmann K (2012) Anoctamins are a family of Ca^{2+}-activated Cl^- channels. J Cell Sci doi: 10.1242/jcs.109553.

Tien J, Lee HY, Minor DL, Jr., Jan YN, Jan LY (2013) Identification of a dimerization domain in the TMEM16A calcium-activated chloride channel (CaCC). Proc Natl Acad Sci U S A 110(16):6352-6357.

Wang M, Yang H, Zheng LY, Zhang Z, Tang YB, Wang GL, Du YH, Lv XF, Liu J, Zhou JG, Guan YY (2012) Downregulation of TMEM16A calcium-activated chloride channel contributes to cerebrovascular remodeling during hypertension by promoting basilar smooth muscle cell proliferation. Circulation 125(5):697-707.

Wang Q, LargeWA. (1993) Action of histamine on single smooth muscle cells dispersed from the rabbit pulmonary artery. *J Physiol* 68: 125-139.

Wagner JA, Cozens AL, Schulman H, Gruenert DC, Stryer L, Gardner P (1991) Activation of chloride channels in normal and cystic fibrosis airway epithelial cells by multifunctional calcium/calmodulin-dependent protein kinase. *Nature* 349:793–96

Wasserman MA, Mukherjee A (1988) Regional differences in the reactivity of guinea-pig airways. *Pulm. Pharmacol.*1:125–31

Wijeong Jang, Ji Young Kim, Shanyu Cui, Juyeon Jo, Byoung-Cheol, Yeonwoo Lee, Ki-Sun Kwon, Chul-Seung Park, and Changsoo Kim (2015) The Anoctamin Family Channel Subdued Mediates Thermal Nociception in *Drosophila*. J Biol Chem M114.592758.

Whitlock JM, and Hartzell C (2016) A Pore Idea: the ion conduction pathway of TMEM16/ANO proteins is composed partly of lipid. *Pflugers Arch.* 468:455–473. http ://dx .doi .org /10.1007 /s00424 -015 -1777 -2

Worrell RT, Frizzell RA (1991) CaMKII mediates stimulation of chloride conductance by calcium in T84 cells. *Am. J. Physiol.Cell Physiol.* 260:C877–82

Xiao Q, Kuai Y, Patriciaperez-Cornejo, Yuanyuan C, Jorge Arreola, and Hartzell C (2011) Voltage- and calcium-dependent gating of TMEM16A/Ano1 chloride channels are physically coupled by the first intracellular loop. Proc Natl Acad Sci U S A **108**, 8891-8896.

Xiao Q, Cui Y (2014) Acidic amino acids in the first intracellular loop contribute to voltage- and calcium- dependent gating of anoctamin1/TMEM16A. PLoS One 9(6):e99376.

Xie W, Kaetzel MA, Bruzik KS, DedmanJR, Shears SB, Nelson DJ (1996) Inositol 3,4,5,6-tetrakisphosphate inhibits the calmodulin-dependent

protein kinase II-activated chloride conductance in T84 colonic epithelial cells. *J. Biol. Chem.*271:14092–97.

Xie W, Kaetzel MA, Bruzik KS, DedmanJR, Shears SB, Nelson DJ (1998) Regulation of Ca^{2+}-dependent Cl^- conductance in a human colonic epithelial cell line (T84): cross-talk between Ins(3,4,5,6)P4 and protein phosphates. *J.Physiol.* 510.3:661–73.

Xiong LW, Kleerekoper QK, Wang X&Putkey JA. (2010) Intra- and interdomain effects due to mutation of calcium-binding sites in calmodulin. *J Biol Chem* 285, 8094-8103.

Xiu Ming Wong, Susan Younger, Christian J Peters, Yuh Nung Jan, Lily Y Jang (2013) Subdued, a TMEM16 family Ca^{2+}-activated Cl- channel in *Drosophila melanogaster* with an unexpected role in host defense. *eLife* 2013;2:e00862.

Yang H, Kim A, David T, Palmer D, Jin T, Tien J, Huang F, Cheng T, Coughlin SR, Jan YN, Jan LY (2012) TMEM16F forms a Ca^{2+}-activated cation channel required for lipid scrambling in platelets during blood coagulation. Cell 151:111-112.

Yang YD, Cho H, Koo JY, Tak MH, Cho Y, Shim WS, Park SP, Lee J, Lee B, Kim BM, Raouf R, Shin YK, Oh U (2008) TMEM16A confers receptor-activated calcium-dependent chloride conductance. *Nature* 455: 1210-1215.

Yu K, Duran C, Qu Z, Cui YY, Hartzell HC (2012) Explaining calcium-dependent gating of anoctamin-1 chloride channels requires a revised topology. Circ Res 110(7):990-999.

국문초록

세포 내 Ca^{2+}에 의해 활성화되는 Calcium activated Chloride Channel (CaCC)는 매우 다양한 조직과 세포들에서 발현되며 전해질, 이온, 물 및 각종 소화효소 등의 분비, 감각신경신호의 증폭, 심장의 흥분 조절과 같은 여러 생리학적 현상 및 질병들에서 매우 중요한 역할들을 관여한다고 알려져 있다. 최근에 이러한 생리학적인 역할을 수행하는 CaCC 유전자로서 이 CaCC 의 전기생리학적, 약물학적 특징들을 보여줌으로 강력한 후보 단백질로 알려지게 되었다. ANO1 에 대한 연구들 중에서도 특히 세포 내 Ca^{2+} 결합부위의 결정과 그 활성화 기전을 밝히기 위한 연구들이 많이 진행되고 있지만 그 정확한 부위와 기전에 대해 아직 명확하게 밝혀지지 않고 있다. 이번 실험에서는 ANO1 의 활성과 관련된 특징들을 가진 페밀리들을 선별한 후, ANO1 과의 염기서열 정렬을 통해 공통의 잠재적인 Ca^{2+} 결합부분들의 변이를 제작한 후 각각의 칼슘 민감성을 확인하였다. 그 결과 ANO1 의 세 번째 세포 내 고리부분이 칼슘 민감성과 밀접한 연관성을 있음을 확인하였고, 단백질 구조예측 프로그램을 이용하여 이 부분이 두 개의 인접한 helix 를 이루는 모델을 예측하였다. 두 helix 중에 음전하를

띄는 단백질을 가진 helix 를 Ca^{2+} sensor helix 라 명명하였고, 이와 상대적인 양전하를 띄는 단백질이 많은 다른 helix 를 reference helix 라고 명명하였다. 이 모델을 토대로 단백질 이차 구조결정 방법 및 분자들 간의 상호 작용을 알아보는 실험을 통하여 두 개의 helix 가 정전기적인 인력을 통해 결합하고 있으며, 두 helix 사이의 결합은 Ca^{2+}에 의해 상쇄되는 것을 확인할 수 있었다. 또한 ANO1 과 ANO2 에 Ca^{2+} sensor helix 와 reference helix 들에 있는 특정전하를 가지는 단백질들의 변이를 만든 후 각각의 칼슘 민감도를 확인한 결과, Ca^{2+} sensor helix 에 특정 glutamate 들이 칼슘 민감도 가장 큰 영향을 미치고, reference helix 는 여러 개의 양전하를 가지는 단백질들을 중성화시키거나 helix 자체를 제거하였을 때 칼슘 민감도가 감소하는 것을 확인하였다. 더욱이 ANO1 의 다른 활성물질인 E_{act} 화합물에 의한 ANO1 의 활성이 reference helix 에서 조절되는 것을 확인하였다. 하지만, 또 다른 ANO1 을 활성 시키는 고전압과 높은 온도에 의한 활성은 두 개의 helix 에서 영향을 받지 않는 것을 확인하였다. 이를 통해, ANO1 이 평상시에는 세 번째 세포 내 고리 내에 두 개의 helix 가 결합하고 있다가 세포 내 Ca^{2+} 증가함에 따라, 증가된 Ca^{2+}이 Ca^{2+}sensor helix 에 결합하고, 이를 통해 기존에 결합된 reference helix 와의 정전기적 인력이 약해지면서 Ca^{2+} sensor helix 움직이는 Ca^{2+} 에

의존적인 밀고 당기는 구조적 변화 (Ca^{2+} dependent push-pull conformational change)의 새로운 활성화 기전을 제시하였다.